Aus dem Pathologischen Institut
der Ludwig-Maximilians-Universität München
Direktor: Prof. Dr. med. Thomas Kirchner

Therapeutic targeting of tumor cell plasticity in colorectal cancer

---

Dissertation zum Erwerb des
Doktorgrades der Naturwissenschaften (Dr. rer. nat.)
an der Medizinischen Fakultät
der Ludwig-Maximilians-Universität München

vorgelegt von

Eva Marina Schmidt

aus München

2018

Gedruckt mit der Genehmigung der Medizinischen Fakultät

der Ludwig-Maximilians-Universität München

Betreuer:	Prof. Dr. rer. nat. Andreas Jung
Zweitgutachter:	Prof. Dr. rer. nat. Roland Kappler
Dekan:	Prof. Dr. med. dent. Reinhard Hickel
Tag der mündlichen Prüfung:	19.12.2018

Meiner Familie

EIDESSTATTLICHE VERSICHERUNG

Ich erkläre hiermit an Eides statt, dass ich die vorliegende Dissertation mit dem Thema

„ Therapeutic targeting of tumor cell plasticity in colorectal cancer “

selbständig verfasst, mich außer der angegebenen keiner weiteren Hilfsmittel bedient und alle Erkenntnisse, die aus dem Schrifttum ganz oder annähernd übernommen sind, als solche kenntlich gemacht und nach ihrer Herkunft unter Bezeichnung der Fundstelle einzeln nachgewiesen habe.

Ich erkläre des Weiteren, dass die hier vorgelegte Dissertation nicht in gleicher oder in ähnlicher Form bei einer anderen Stelle zur Erlangung eines akademischen Grades eingereicht wurde.

München, 20.06.2018

Eva Marina Schmidt

PUBLICATIONS

Parts of this thesis have been published in:

- **Schmidt, E. M.,** Lamprecht, S., Blaj, C., Schaaf, C., Krebs, S., Blum, H., Hermeking, H., Jung, A., Kirchner, T. & Horst, D. Targeting tumor cell plasticity by combined inhibition of NOTCH and MAPK signaling in colon cancer. *J. Exp. Med.* **215**, 1693-1708 (2018).

In addition, I contributed to the following publications, which are not further described in this thesis:

- Lamprecht, S. *, Kaller, M. *, **Schmidt, E. M.,** Blaj, C., Schiergens, T. S., Engel, J., Jung, A., Hermeking, H., Grünewald, T. G. P., Kirchner, T. & Horst, D. PBX3 is part of an EMT regulatory network and indicates poor outcome in colorectal cancer. *Clin. Cancer Res.* **24**, 1974-1986 (2018). * Authors contributed equally to this work.

- Lamprecht, S., **Schmidt, E. M.,** Blaj, C., Hermeking, H., Jung, A., Kirchner, T. & Horst, D. Multicolor lineage tracing reveals clonal architecture and dynamics in colon cancer. *Nat. Commun.* **8**, 1-9 (2017).

- Blaj, C., **Schmidt, E. M.,** Lamprecht, S., Hermeking, H., Jung, A., Kirchner, T. & Horst, D. Oncogenic effects of high MAPK activity in colorectal cancer mark progenitor cells and persist irrespective of RAS mutations. *Cancer Res.* **77**, 1763-1774 (2017).

- Blaj, C., Bringmann, A., **Schmidt, E. M.,** Urbischek, M., Lamprecht, S., Fröhlich, T., Arnold, G. J., Krebs, S., Blum, H., Hermeking, H., Jung, A., Kirchner, T. & Horst, D. ADNP is a therapeutically inducible repressor of WNT signaling in colorectal cancer. *Clin. Cancer Res.* **23**, 2769-2780 (2017).

- Woischke, C.*, Blaj, C.*, **Schmidt, E. M.***, Lamprecht, S., Engel, J., Hermeking, H., Kirchner, T. & Horst, D. CYB5R1 links epithelial-mesenchymal transition and poor prognosis in colorectal cancer. *Oncotarget* **7**, 31350-31360 (2016). * Authors contributed equally to this work.

CONTENTS

1 INTRODUCTION

1.1 Colorectal cancer

1.1.1 Epidemiology

Cancer is one of the leading public health problems worldwide with 17.5 million new cases recorded in 2015 [1,2]. Among those, colorectal cancer (CRC) is the third most common cancer in males and the second most frequent in females [2], and is a major cause of cancer mortality [3,4]. The risk of developing CRC is associated with a number of dietary and lifestyle factors, including alcohol consumption, smoking, diet rich in red meat, and reduced physical activity [3,5]. CRC-caused mortality is decreasing due to progress in CRC screenings, enhanced awareness in diet and lifestyle, as well as improvements in cancer therapy [5,6]. However, the number of CRC-related deaths with 835,000 in 2015 remains a social burden [2]. Hence, further research is needed to develop new concepts for therapy in order to increase survival rates of patients with CRC.

1.1.2 Genetic background and hallmarks of cancer

The development of CRC is a multistep process involving mutational changes in the genome [7–9]. For transformation of colon epithelial cells into malignant cancer cells, at least four to five mutations in so called driver genes are required [8], which mediate a selective growth advantage [10]. Driver gene mutations typically either activate oncogenes or cause loss of function of tumor suppressor genes, both contributing to tumor formation [9]. The main genetic alterations and their occurrence during colorectal tumorigenesis are described in the adenoma-carcinoma sequence model, which was proposed by Fearon and Vogelstein [8] (Figure 1).

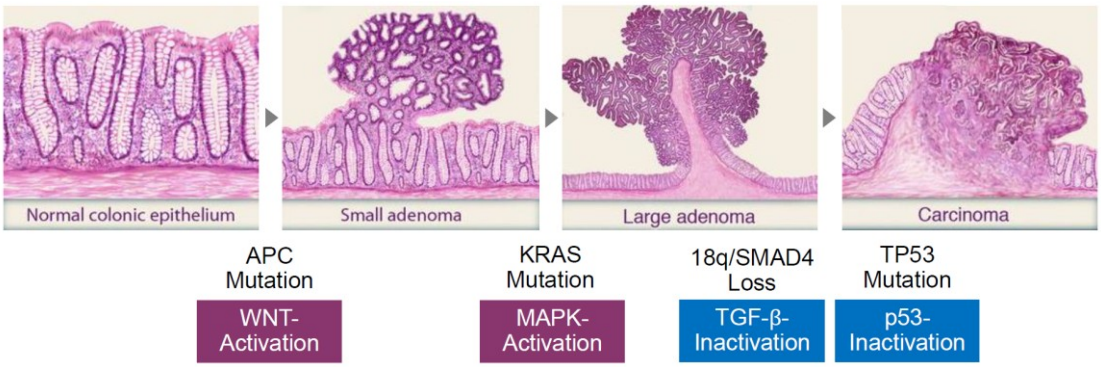

Figure 1. Adenoma-carcinoma sequence model.

Representative H&E stained sections of normal colon epithelium, small and large adenoma, and carcinoma. Driver gene mutations acquired during carcinogenesis and corresponding pathway alterations are indicated below. Figure was adapted from references [8,10].

The first driver gene mutations often arise in *Adenomatous polyposis coli* (*APC)* [7,10,11], leading to transformation of normal mucosa into small adenomas [7] (Figure 1). *APC* mutations are observed in approximately 70-80 % of sporadic colorectal adenomas and carcinomas [4], and are crucial for tumor initiation [7]. For malignant transformation, further mutations in other driver genes are required [7,10,11]. The *KRAS* gene is mutated in about 50 % of adenomas larger than 1 cm [4,12], and mutated KRAS contributes to the expansion of preexisting adenomas [10,13] (Figure 1). Also, loss of heterozygosity (LOH) on chromosome 18q is found in more than 70 % of CRC [4,12]. Due to 18q LOH, mutations in the *SMAD4* gene may emerge, which are associated with advanced stages of malignant transformation [14,15] (Figure 1). Furthermore, mutations in the *TP53* gene may arise, which are mainly detectable in carcinomas with an estimated frequency of 60 % [11,12] (Figure 1). These four driver gene mutations are highly frequent in CRC and often occur within the adenoma-carcinoma sequence [8,12].

Accumulated driver gene mutations synergistically induce the development of essential functional capabilities, transmitting selective growth advantages to mutated epithelial cells and thus foster colorectal tumor development and cancer progression [9,16]. The acquired capabilities, such as sustained proliferation and evasion of apoptosis, are not only relevant to CRC but are common features of most

types of human cancer and were referred to as the hallmarks of cancer by Hanahan and Weinberg in 2000 [9] (Figure 2).

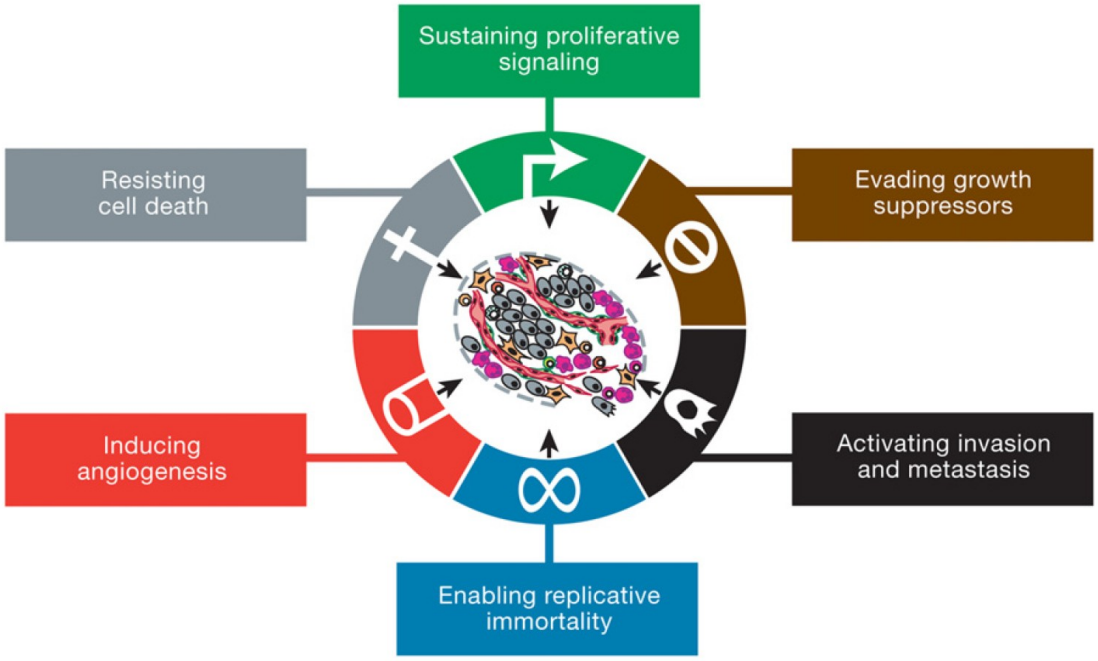

Figure 2. The hallmarks of cancer.
Functional capabilities of human cancer acquired during tumor development. Figure was adapted from reference [16].

Additional capabilities of cancer cells, such as the induction of angiogenesis, replicative immortality, and the activation of invasion and metastasis further contribute to carcinogenesis [16] (Figure 2). These hallmarks of cancer are often influenced by the aberrant activation or inactivation of distinct signaling pathways, which is frequently caused by mutations in the mentioned driver genes *APC*, *KRAS*, *SMAD4* and *TP53* [9].

1.2 Signaling-pathway alterations in colorectal cancer

1.2.1 The WNT pathway

In this context, the WNT pathway appears to assume a central role in tumor initiation of CRCs [17,18]. Aberrant WNT signaling is induced by *APC* mutations causing the functional loss of the tumor suppressor protein APC. Under physiological conditions, APC serves as a negative regulator of β-catenin, which is part of the canonical WNT signaling pathway [19]. Upon APC loss, β-catenin accumulates in the nucleus and forms a stable complex with the transcription factor TCF4. This induces constitutive transcriptional activation of WNT target genes [17,20] (Figure 1). Intestinal epithelial cells with persistent WNT-signaling activity then are shifted into a proliferative phenotype with simultaneous blockage of terminal differentiation [9,20,21]. Thus, APC-mutated intestinal epithelial cells may selectively expand, which is the basis for adenoma formation [18,21]. Despite the presence of APC mutations within all tumors cells of a CRC, WNT signaling is heterogeneously activated within most of these tumors [22,23]. Specifically, active WNT signaling is frequently detectable in tumor cells at the infiltrative tumor edge [22,24]. On the contrary, colon cancer cells located more centrally within the tumor have a comparatively low activity for this pathway [22,24,25].

1.2.2 The Mitogen-activated protein kinase pathway

Further pathway alterations often occur in the mitogen-activated protein kinase (MAPK)-signaling pathway, which seems to be associated with tumor progression of CRCs [26]. The MAPK signaling pathway is a key regulator of normal cell proliferation, differentiation, survival, and motility [27,28]. Pathway activity is mediated by MAPKs, a family of evolutionarily conserved kinases that transmit signals from extracellular stimuli into specific intracellular responses [27,29]. This signaling pathway involves different MAPK cascades, among which the RAS-RAF-MEK-ERK cascade plays a crucial role in CRC [30–32] (Figure 3).

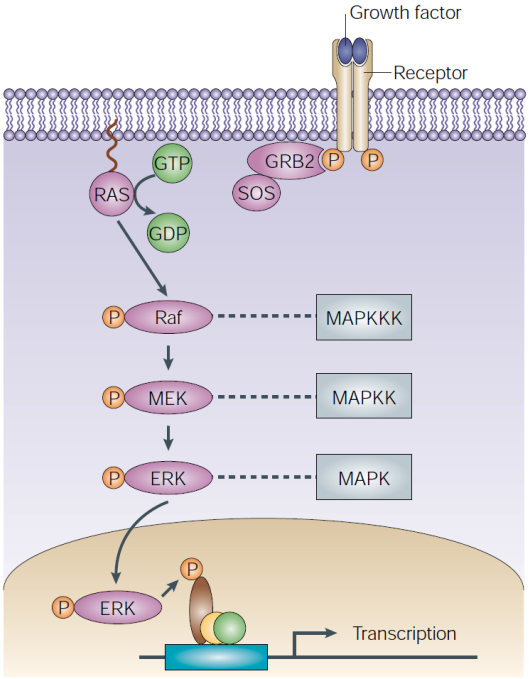

Figure 3. The RAS-RAF-MEK-ERK cascade.

Upon growth factor binding, the receptor is activated and adaptor proteins are recruited to the intracellular domains. Adaptor proteins shift RAS proteins to the guanosine triphosphate (GTP) bound state for activation. RAS-GTP activates RAF (MAPKKK), which in turn phosphorylates and activates MEK (MAPKK). MEK further catalyzes the phosphorylation of ERK (MAPK), which translocates to the nucleus to phosphorylate transcription factors and effector proteins, and thus contributes to target-gene transcription. Figure was adapted from reference [33].

The RAS-RAF-MEK-ERK cascade is activated by growth factor binding to tyrosine kinase receptors, e.g. the epidermal growth factor receptor (EGFR) located at the cell membrane [31,34] (Figure 3). Upon receptor activation, the intracellular domains of the receptor are autophosphorylated and subsequently the adaptor proteins GRB2 and SOS are recruited [28,34]. These proteins then activate RAS proteins such as KRAS by shifting inactive RAS bound to guanosine diphosphate (GDP) to its active guanosine triphosphate (GTP)-bound state [35,36]. RAS-GTP stimulates RAF, a MAPK kinase kinase, which in turn phosphorylates and thereby activates MEK (MAPK kinase) (Figure 3). MEK further catalyzes the phosphorylation of the MAPK extracellular signal-regulated kinase (ERK) [33,34,36]. Following this, activated ERKs translocate to the nucleus phosphorylating and activating various transcription factors and effector proteins [31,33,34] (Figure 3). For instance, the transcription factor JUN is phosphorylated by ERK and subsequently complexes with the protein FOS to form the activator protein 1 (AP1) transcription factor [35,37]. The gene *FOSL1*, as part of the AP1

transcription factor family, encodes FOS-related antigen 1 (FRA1), which is an indicator for MAPK pathway activity [38].

In CRC, mutations in the driver gene *KRAS* lead to the activation of the MAPK-signaling pathway [4,11] (Figure 1). In mutated cancer cells, KRAS accumulates in the active GTP-bound state leading to increased activity of its downstream signaling cascade [36,39,40]. Findings suggest that this aberrant MAPK activity facilitates sustained proliferation of mutated colon cancer cells [16,41] and thereby may contribute to the formation of large villous adenomas [10] (Figure 1). Similar to WNT pathway activity, MAPK signaling is mainly active in colon cancer cells at the infiltrative tumor edge and is characterized by elevated levels of the transcription factor FRA1 [26,38,42].

1.2.3 The transforming growth factor-β-signaling pathway and the p53 protein

In addition, anti-proliferative signals that contribute to tissue homeostasis in normal tissue, may be deregulated in CRC [43]. The transforming growth factor-β (TGF-β)-signaling pathway, a major regulator of growth inhibition in epithelial cells, can be affected by mutations in *SMAD4* [11,15,44] (Figure 1). Normally, the SMAD4 protein transmits TGF-β receptor signaling to the nucleus, which induces expression of TGF-β responsive genes [9,43]. Mutational inactivation of SMAD4 may disrupt signal transduction and facilitates cell proliferation and malignant progression of CRC [14,15].

Besides promotion of growth, colon cancer cells acquire the ability to evade programmed cell death, also referred to as apoptosis [9]. One of the main mechanisms is the functional inactivation of p53 proteins, which is a result of mutations in the tumor suppressor gene *TP53* [9,45] (Figure 1). The p53 protein is a key sensor of DNA damage and induces cell apoptosis upon genomic abnormalities [4,9,45]. Loss of p53 function mediates resistance towards apoptosis and therefore may facilitate continued growth of mutated colon cancer cells. Furthermore, inactivation of p53 protein may promote the acquisition of invasive characteristics enabling tumor cells to

detach from the primary tumor mass and to migrate to distant sites in the body, which is the basis for metastases formation [4,9].

1.2.4 The NOTCH pathway

Also, the NOTCH signaling pathway is highly active in CRC and appears to contribute to tumor progression. However, in contrast to other signaling pathways, mutations in NOTCH genes are rarely present [46–48]. Basically, the canonical NOTCH signaling cascade is an evolutionarily conserved pathway that plays crucial roles in embryonic development, cell fate decisions, and tissue homeostasis [49–51]. This pathway involves NOTCH receptors as well as two groups of NOTCH ligands termed Delta-like ligands and Jagged ligands, which are located on neighboring cells [21,46,52]. NOTCH signaling is activated by cell-to-cell contact, mediating the interaction of the NOTCH receptors extracellular ligand-binding domains to their ligands [53–55] (Figure 4).

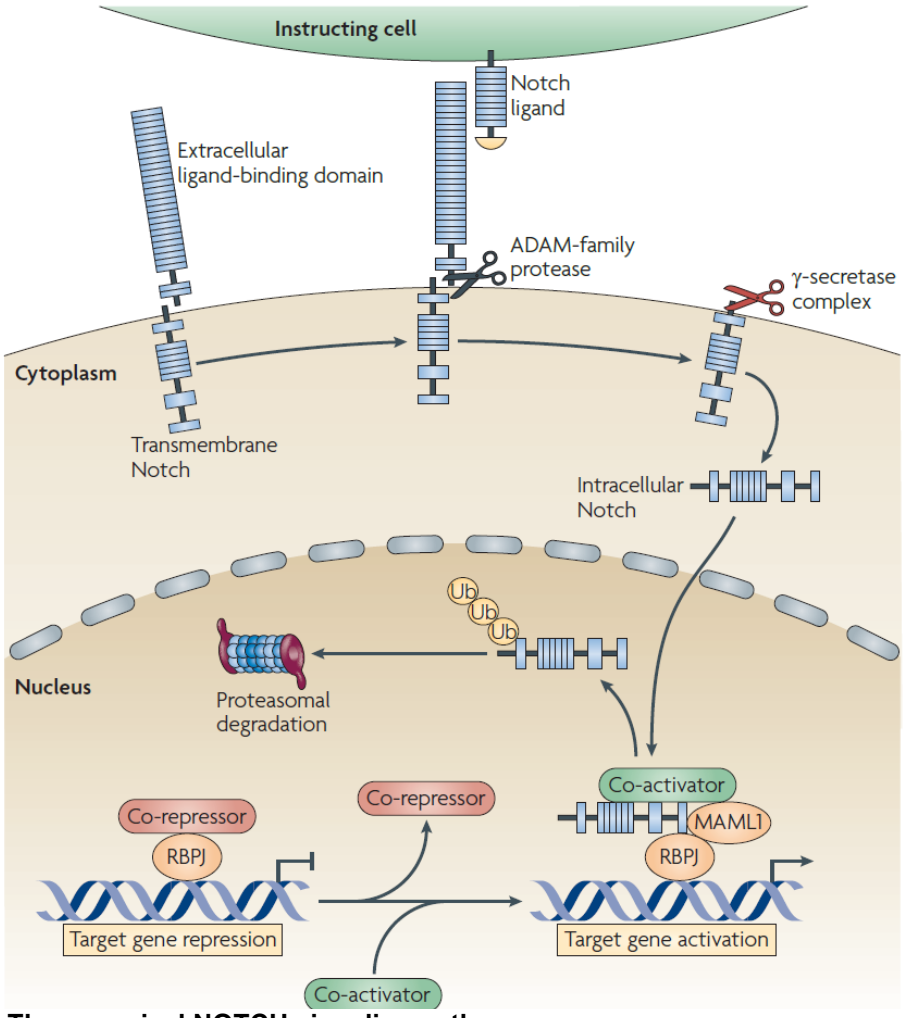

Figure 4. The canonical NOTCH signaling pathway.

NOTCH signaling is activated by the interaction of the NOTCH receptor extracellular ligand-binding domain to its ligand, inducing proteolytic cleavages of the NOTCH receptor. The extracellular domain is cleaved off by an ADAM (a disintegrin and metalloproteinase) family protease. Cleavage by a γ-secretase complex then results in the release of the active NOTCH intracellular domain (NICD) and its translocation to the nucleus. There, NICD complexes with the transcription factor recombination-signal-binding protein for immunoglobulin-κ J region (RBPJ) followed by the recruitment of Mastermind-like protein 1 (MAML1) and further co-activators. This activation complex induces NOTCH target-gene transcription. NICD activity is terminated by ubiquitin-mediated protein degradation. Figure was adapted from reference [56].

Ligand binding induces two consecutive proteolytic cleavages of the NOTCH receptor [49,52,57]. First, an ADAM (a disintegrin and metalloproteinase) family protease catalyzes the removal of the NOTCH extracellular domain [57,58]. The second cleavage by a γ-secretase complex then releases the active NOTCH intracellular domain (NICD) into the cytoplasm [53,59,60] (Figure 4). Following this, NICD translocates to the nucleus and complexes with the transcription factor recombination-signal-binding protein for immunoglobulin-κ J region (RBPJ) that is bound to the promoter of NOTCH target genes [46,56,61]. Upon NICD-RBPJ binding, the transcriptional-repressor complex is converted into an activation complex followed by the recruitment of

Mastermind-like protein 1 (MAML1) and further co-activators [54,61,62] (Figure 4). Consequently, the transcription of NOTCH target genes is activated. Among those, genes encoding members of the Hairy Enhancer of Split (HES) family such as HES1 are the most common ones [21,46]. NOTCH signaling activity is terminated by ubiquitin-mediated protein degradation of NICD [54,56] (Figure 4).

In CRC, the NOTCH signaling pathway is often hyperactive, which is thought to be caused by aberrant expression of NOTCH ligands such as JAGGED1 and mutations in negative regulators of the NOTCH pathway [46,54]. Active NOTCH signaling seems to affect a number of tumor-promoting functions in CRC. Intestinal tumor initiation, for example, requires active NOTCH signaling mediated by increased levels of JAGGED1 [63–65]. High NOTCH activity has also been linked to cancer stem cell phenotypes [66,67] and to EMT [68,69], both contributing to the function of NOTCH signaling in tumor progression [70,71]. However, contradictory findings also were reported and suggested that NOTCH activity represses the expression of WNT target genes in human colorectal cancer cells [72]. Furthermore, the intratumoral distribution of NOTCH activity and associations with distinct tumor cell phenotypes yet are poorly characterized. The exact role of the NOTCH pathway in CRC therefore requires further elucidation.

In summary, several signaling pathways are deregulated in CRC, often through mutations in pathway components. However, most signaling pathways appear to be heterogeneously activated within these tumors, despite the presence of identical driver mutations within all tumor cells of a CRC [22,24,26]. This may be linked to the occurrence of different colon cancer cell phenotypes, which include tumor cells undergoing epithelial-mesenchymal transition (EMT) and colon cancer stem cells.

1.3 Epithelial-mesenchymal transition

Activation of invasion and metastasis is one of the hallmarks of cancer and is regulated by a molecular and cellular program termed EMT [16]. Besides its physiological involvement in organ development and wound healing, EMT plays a role in tissue fibrosis and cancer progression [73]. During EMT, cancer cells undergo a phenotypic shift from an epithelial to a mesenchymal state that is characterized by loss of cell-cell adhesion and apical-basal polarity, changes in cell shape towards spindle-like morphology, and acquisition of motility and invasive features [74–77]. In the context of tumor progression, cancer cells with activated EMT are able to detach from the primary tumor mass, invade surrounding tissues, and may enter the systemic circulation [75,77] (Figure 5, a and b).

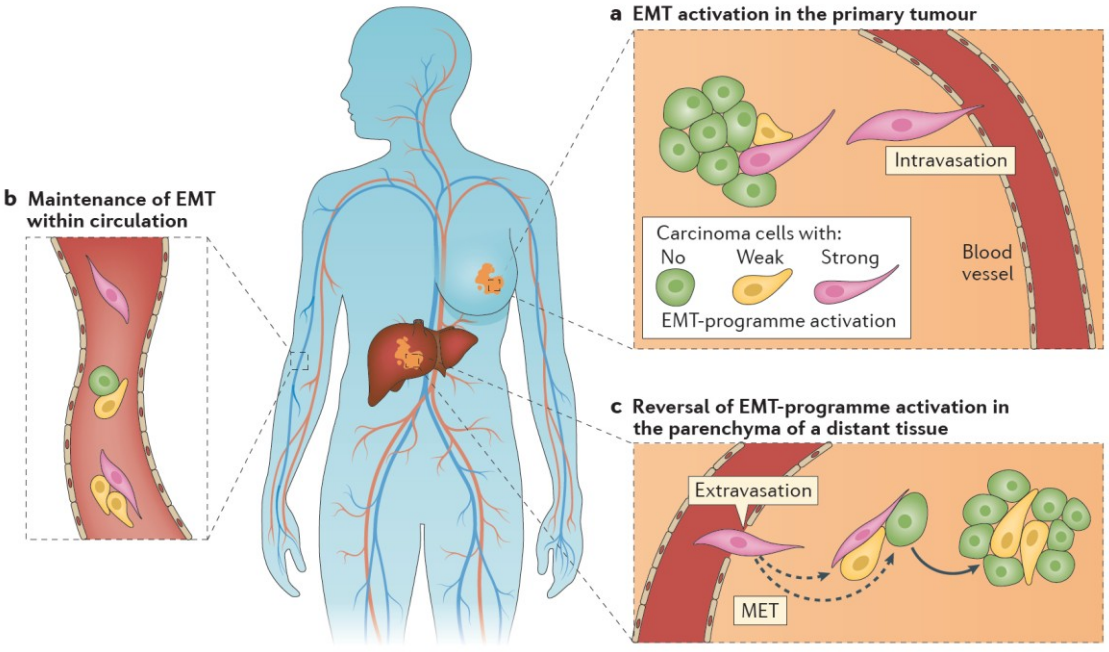

Figure 5. EMT program activation during carcinoma progression.

(a) Activation of EMT enables cancer cells to detach from the primary tumor, invade the surrounding tissue and intravasate. **(b)** EMT is maintained in cancer cells within circulation. **(c)** Following extravasation, cancer cells undergo mesenchymal-epithelial transition (MET), the reversal of EMT, to colonize distant tissue and form macroscopic metastases. Figure and figure legend were adapted from reference [77].

Following transportation to distant sites, cancer cells with maintained mesenchymal phenotype extravasate to the tissue parenchyma [77]. However, to colonize these tissues and form macroscopic metastases, cancer cells may return to an epithelial

state by a reverse process termed mesenchymal-epithelial transition (MET) [77–79] (Figure 5 c). The reversibility of the EMT program, including EMT as well as MET, implies substantial phenotypic plasticity of cancer cells. Findings suggest that this plasticity contributes to metastasis formation and is discussed as a possible mechanism for evading cancer therapy [77,80].

The phenotypic shift of colon cancer cells during EMT is based on a number of molecular changes. The loss of E-cadherin as the main adherens junction protein in epithelia represents a crucial step in the initiation of the mesenchymal state [74,75,81]. To further stabilize this phenotype, mesenchymal markers such as Fibronectin and Vimentin are upregulated [73,77]. The shift from epithelial to mesenchymal states is mediated by EMT-inducing transcription factors, such as SNAI1, SNAI2, ZEB1 and ZEB2, that activate or repress the transcription of EMT-associated genes [73,77,82]. The *CDH1* gene encoding E-cadherin is a key transcriptional target of these EMT regulators [16,73,75], which directly bind to E-box sequences on the promoter of *CDH1* leading to its transcriptional repression [83–88].

For EMT induction in CRC, these transcription factors are activated by multiple signaling pathways [73,76,89]. For instance, WNT-signaling activity induces the expression of ZEB1 and thus may contribute to EMT and the resulting invasive phenotype of colon cancer cells [90]. Further studies suggest that MAPK signaling activity also contributes to EMT by increasing the levels of FRA1 [42,73], which directly targets EMT-related genes and thus may contribute to the mesenchymal phenotype of colon cancer cells as well as to tumor cell plasticity [38,42].

Within CRC, cancer cells with mesenchymal traits are located predominantly at the infiltrative tumor edge, whereas cancer cells towards the center often reveal a more epithelial-like phenotype [22,91]. The distinct phenotypes of colon cancer cells can be assessed by the expression of phenotypic markers. One such marker is the

WNT-target LAMC2, which is mainly expressed in invading colon cancer cells at the tumor edge and indicates EMT [90–92]. Additionally, the expression of the epithelial marker E-cadherin is reduced in those cells in contrast to cancer cells in the tumor center [26,77].

To sum up, the EMT program is a major regulator of invasive cancer growth and metastasis formation. Due to its implied contribution to phenotypic plasticity of colon cancer cells, therapeutic targeting of the EMT program may be a promising approach for the development and improvement of cancer treatment.

1.4 Colorectal cancer stem cells

The distinct colon cancer cell phenotypes within CRC further comprise cancer cells with stem-like properties, which are defined as cancer stem cells (CSCs) [74]. In addition to the abilities of self-renewal and tumor initiation, these cells were suggested to be capable of differentiating into less-tumorigenic cancer cells forming the tumor mass [77,93,94]. In solid tumors, CSCs are thought to represent a relatively small tumor cell subpopulation that together with the more differentiated progeny cells contributes to intratumoral phenotypic heterogeneity [76,77,95,96].

In CRC, putative CSCs were identified by different cell markers, such as CD133, nuclear β-catenin, and leucine-rich repeat-containing G protein-coupled receptor 5 (LGR5) [97–99]. Furthermore, colorectal CSCs seem to be located at the infiltrative tumor edge, whereas more differentiated tumor cells are found in the tumor center [24,91]. To characterize cancer stem cells within tumors, lineage tracing approaches were recently developed [100,101]. These approaches genetically labeled single tumor cells, e.g. by a fluorescent dye. By transmitting this genetic, fluorescent label to all progeny cells, expanding clones of tumor cells formed and cells originating from a single tumor cell could be identified [102]. Using a lineage tracing approach, Schepers *et al*. identified LGR5 expressing colon cancer cells as a cell subpopulation, driving intestinal tumor progression [100]. The capability of specific cancer cells to differentiate into phenotypically distinct tumor cell subpopulations may confirm the existence of colorectal CSCs [94,98–100]. Further findings suggest that less-tumorigenic epithelial cancer cells have the ability to dedifferentiate into colorectal CSCs. This implies a plasticity between those cancer cell subpopulations [103,104]. Moreover, the EMT program mentioned above appears to be closely linked to cancer stem cell phenotypes, as the activation of EMT may increase stem-like properties of cancer cells [105,106].

Tumor cell subpopulations with EMT and CSC phenotypes may have clinical importance due to their potential resistance against standard chemotherapy that appears to mainly target proliferating cancer cells of the more differentiated tumor mass [77,91,95,107]. Targeted therapies against such tumor cell subpopulations with high activities of oncogenic signaling pathways thus may be a promising approach to increase the efficacy of anticancer therapy and to improve personalized medicine in CRC.

1.5 Treatment of colorectal cancer

1.5.1 Surgery and chemotherapy

In early stages of CRC, the complete surgical removal of the tumor may be curative [108], whereas the treatment of advanced disease additionally relies on systemic therapy. Adjuvant chemotherapy improves patients' survival rates and is the clinical standard treatment of advanced CRC [108–110]. When surgery and adjuvant chemotherapy become insufficient [68], the use of biologically active agents that target oncogenic signaling pathways, such as MAPK and NOTCH signaling, may be another treatment option in patients with advanced CRC [68,111].

1.5.2 Targeted therapy against oncogenic signaling pathways

Owing to the frequent activation of MAPK signaling in cancer and its contribution to tumor progression, targeting MAPK signaling by blocking EGFR with therapeutic antibodies such as cetuximab is a commonly used approach [74,112,113]. In human CRC cell lines, cetuximab only inhibits MAPK signaling in cells without *KRAS* mutations [114]. Furthermore, colorectal cancers often develop resistance to cetuximab therapy, which is associated with acquired *KRAS* mutations [115]. In the clinical setting, treatment with cetuximab improves overall and progression-free survival of patients, whereas the therapeutic success is restricted to *KRAS* wild-type CRC [114,116–118]. As *KRAS* mutations are highly frequent in CRC and are associated with poor survival in patients with advanced CRC [26,119,120], therapeutic regimens for KRAS mutated CRC are of great demand [121]. A potential KRAS downstream target may be MEK, which can be inhibited by the use of MEK inhibitors [27,36,122]. Selumetinib (AZD6244) is a potent and selective MEK inhibitor with antitumor activity that has the ability to prevent ERK phosphorylation regardless of the KRAS mutation status [28,114,122]. Furthermore, selumetinib is clinically evaluated. To date, treatment of advanced CRC

with selumetinib as single agent prolongs stable disease, however, these beneficial effects are limited [123,124].

Besides targeting MAPK signaling, the NOTCH pathway might be a promising therapeutic target due to its aberrant activation and its predominant tumor-promoting functions. The most common agents are γ-secretase inhibitors such as dibenzazepine (DBZ), which block the γ-secretase-mediated proteolytic cleavage of the NOTCH receptor and thus prevent the release of NICD [49,54]. In preclinical studies, single γ-secretase inhibitor treatment reduced colon cancer cell proliferation, tumor formation as well as tumor growth [125,126]. By contrast, other studies demonstrated no beneficial effects of single agent treatment, whereas the combination of γ-secretase inhibitors and chemotherapy increased the treatment response of colon cancer cells [127,128]. In CRC patients, NOTCH1 positivity as well as high levels of HES1 are both associated with poor prognosis [129,130]. Several γ-secretase inhibitors are currently under clinical evaluation and reveal a downregulation of NOTCH target genes in patients with advanced solid tumors [131,132]. Regarding antitumor efficacy, however, single agent treatment with γ-secretase inhibitors was not beneficial for patients with in advanced colon cancers [133,134].

Despite promising results in preclinical studies [114,125], no benefits of single agent treatment with MEK or γ-secretase inhibitors were obtained in the clinical setting, respectively [123,133]. Therefore further research is needed to identify patients that might benefit from targeted therapeutic approaches against active NOTCH and MAPK signaling in CRC.

2 AIMS OF THE STUDY

The present study had the following aims:

- Characterizing NOTCH-signaling activity in colorectal cancer to reveal its intratumoral distribution and associated tumor cell phenotypes

- Evaluating the clinical relevance of tumor cell subpopulations with differential MAPK and NOTCH signaling activity in colorectal cancer

- Determining phenotypic plasticity of colorectal cancer cells with differential phenotypes and pathway activities

- Testing the effects of targeted therapy on tumor cell subpopulations with high MAPK or NOTCH pathway activity, and evaluating related changes on tumor cell phenotypes and tumor growth

3 MATERIALS

3.1 Chemicals and reagents

Reagent	Supplier
4-Hydroxytamoxifen ≥70% Z isomer	Sigma-Aldrich, St. Louis, MO, USA
4x Laemmli Sample Buffer	Bio-Rad, Munich, Germany
Acetic acid 100 %	Carl Roth GmbH, Karlsruhe, Germany
Agarose Biozym LE	Biozym Scientific, Hessisch Oldenforf, Germany
Albumin Fraction V	Carl Roth GmbH, Karlsruhe, Germany
All-purpose Hi-Lo DNA Marker	Bionexus Inc., Oakland, CA, USA
Ammonium peroxodisulfate	Carl Roth GmbH, Karlsruhe, Germany
Ammonium sulphate	Carl Roth GmbH, Karlsruhe, Germany
Ampicillin sodium salt	Sigma-Aldrich, St. Louis, MO, USA
Antibody diluent	Agilent, Santa Clara, CA, USA
β-Mercaptoethanol	Bio-Rad, Munich, Germany
Aqua ad iniectablia	Deltamedica GmbH, Reutlingen; Germany
Biofreeze freezing medium	Biochrom, Berlin, Germany
Blasticidin	Carl Roth GmbH, Karlsruhe, Germany
cOmplete™, Mini Protease Inhibitor Cocktail	Roche Diagnostics GmbH, Penzberg, Germany
DAPI (4′,6-Diamidin-2-phenylindol)	Carl Roth GmbH, Karlsruhe, Germany
Deoxycholic acid sodium salt	Carl Roth GmbH, Karlsruhe, Germany
Dibenzazepine	Axon Medchem BV, Groningen, The Netherlands
Dimethylsulfoxide	Carl Roth GmbH, Karlsruhe, Germany
dNTP Mix	Thermo Fisher Scientific Inc., Waltham, MA, USA
DMEM	Biochrom, Berlin, Germany
Doxycycline hyclate	Sigma-Aldrich, St. Louis, MO, USA

Reagent	Supplier
Ethylenediaminetetraacetic acid	Sigma-Aldrich, St. Louis, MO, USA
EGF Recombinant Human Protein	Thermo Fisher Scientific Inc., Waltham, MA, USA
Ethidium bromide solution 1%	Carl Roth GmbH, Karlsruhe, Germany
Fetal Bovine Serum	Biochrom, Berlin, Germany
FGF-Basic (AA 10-155) Recombinant Human Protein	Thermo Fisher Scientific Inc., Waltham, MA, USA
Glycine	Carl Roth GmbH, Karlsruhe, Germany
imMedia™ Growth Medium, agar, ampicillin	Thermo Fisher Scientific Inc., Waltham, MA, USA
Immobilon-P PVDF Membrane	Merck Millipore, Billerica, MA, USA
Immobilon Western Chemiluminescent HRP Substrate	Merck Millipore, Billerica, MA, USA
LB Broth (Luria/Miller)	Carl Roth GmbH, Karlsruhe, Germany
Lenti-X Concentrator	Clontech, Mountain View, CA, USA
LipoD293 DNA (Ver. II)	Tebu-bio, Le Perray-en-Yvelines, France
Matrigel	Corning Life Sciences, Tewksbury, MA, USA
Magnesium chloride	Qiagen GmbH, Hilden, Germany
Methanol	Carl Roth GmbH, Karlsruhe, Germany
Methocel (Hydroxypropylmethyl cellulose)	Sigma-Aldrich, St. Louis, MO, USA
Nonidet™ P 40 Substitute	Sigma-Aldrich, St. Louis, MO, USA
PageRuler™ Plus Prestained Protein Ladder	Thermo Fisher Scientific Inc., Waltham, MA, USA
Penicillin/Streptomycin	Biochrom, Berlin, Germany
PhosSTOP™	Roche Diagnostics GmbH, Penzberg, Germany
Polybrene (Hexadimethrine bromide)	Sigma-Aldrich, St. Louis, MO, USA
ProLong™ Gold Antifade Mountant	Thermo Fisher Scientific Inc., Waltham, MA, USA
Protein Block	Agilent, Santa Clara, CA, USA
Puromycin dihydrochloride	Merck Millipore, Billerica, MA, USA
QIAzol Lysis Reagent	Qiagen GmbH, Hilden, Germany

Reagent	Supplier
Rotiphorese® Gel 30 (37,5:1)	Carl Roth GmbH, Karlsruhe, Germany
SDS ultra pure	Carl Roth GmbH, Karlsruhe, Germany
Selumetinib (AZD6244)	Selleckchem, Houston, TX, USA
Skim milk powder	Sigma-Aldrich, St. Louis, MO, USA
Sodium chloride	Carl Roth GmbH, Karlsruhe, Germany
Streptavidin, Alexa Fluor™ 488	Thermo Fisher Scientific Inc., Waltham, MA, USA
Sunflower seed oil from *Helianthus annuus*	Sigma-Aldrich, St. Louis, MO, USA
Tamoxifen	Sigma-Aldrich, St. Louis, MO, USA
Target Retrieval Solution, Citrate pH 6	Agilent, Santa Clara, CA, USA
TEMED	Carl Roth GmbH, Karlsruhe, Germany
TRIS	Carl Roth GmbH, Karlsruhe, Germany
TRIS hydrochloride	Carl Roth GmbH, Karlsruhe, Germany
Triton® X 100	Carl Roth GmbH, Karlsruhe, Germany
TWEEN® 20	Sigma-Aldrich, St. Louis, MO, USA
TWEEN® 80	Sigma-Aldrich, St. Louis, MO, USA

3.2 Enzymes

Enzymes	Supplier
FastAP Thermosensitive Alkaline Phosphatase	Thermo Fisher Scientific Inc., Waltham, MA, USA
HotStarTaq DNA Polymerase	Qiagen GmbH, Hilden, Germany
Klenow Fragment	Thermo Fisher Scientific Inc., Waltham, MA, USA
Restriction endonucleases	Thermo Fisher Scientific Inc., Waltham, MA, USA
T4 DNA Ligase	Thermo Fisher Scientific Inc., Waltham, MA, USA
Trypsin/ EDTA solution (0.05 %/0.02 %)	Biochrom, Berlin, Germany

3.3 Kits

Kits	Supplier
DC™ Protein Assay	Bio-Rad, Munich, Germany
ImmPRESS™ HRP Anti-Rabbit IgG (Peroxidase) Polymer Detection Kit	Vector Laboratories Inc., Burlingame, CA, USA
Liquid DAB+ Substrate Chromogen System	Agilent, Santa Clara, CA, USA
mi-Plasmid Miniprep Kit	Metabion International AG, Planegg, Germany
OptiView DAB IHC Detection Kit	Ventana Medical Systems, Inc., Tucson, AZ, USA
Permanent AP Red Kit	Zytomed Systems GmbH, Berlin, Germany
PureYield™ Plasmid Midiprep System	Promega GmbH, Mannheim, Germany
QIAamp DNA Micro Kit	Qiagen GmbH, Hilden, Germany
Quick Start Bovine Serum Albumin Standard Set	Bio-Rad, Munich, Germany
Rapid DNA Ligation Kit	Thermo Fisher Scientific Inc., Waltham, MA, USA
SENSE mRNA-Seq Library Prep Kit	Lexogen GmbH, Vienna, Austria
StemPro™ hESC SFM	Thermo Fisher Scientific Inc., Waltham, MA, USA
TSA Plus Cyanine 3 System	Perkin Elmer; Waltham; MA, USA
UltraView Universal DAB Detection Kit	Ventana Medical Systems, Inc., Tucson, AZ, USA
Wizard® SV Gel and PCR Clean-Up System	Promega GmbH, Mannheim, Germany

3.4 Oligonucleotides and vectors

3.4.1 Oligonucleotides

Name	Sequence (5'- 3')	Application
EGFP rev	CGTCGCCGTCCAGCTCGACCAG	Sequencing
KRAS fwd	NNNGGCCTGCTGAAAATGACTGAA	PCR, sequencing
KRAS rev	Biotin-TTAGCTGTATCGTCAAGGCACTCT	PCR
KRAS exon 2 rev	TGTGGTAGTTGGAGCT	Sequencing
mCherry rev	GGATGTCCCAGGCGAAGG	Sequencing
WPRE rev	GGGCCACAACTCCTCATAAA	Sequencing

Polymerase chain reaction (PCR). reverse (rev), forward (fwd)

3.4.2 Vectors

Name	Insert	Reference
pcDNA3.1 EYFP-V5	EYFP-V5	[135]
pCMV-dR8.91	Gag-Pol	[136]
pLenti rtTA3G	Reverse tetracycline transactivator 3G	Dominic Esposito
pLenti TetO-CreERT2,	CreERT2	[135]
pLenti Trace	mCherry-FLAG, EYFP-V5	This work
pMD2.G	VSV G	[137]

3.5 Antibodies

3.5.1 Primary antibodies

Antibody	Species/ Clone	Order #	Supplier	WB	IF	IHC
BrdU	Mouse/ IIB5	sc-32323	Santa Cruz		1:100	
β-catenin	Mouse	610154	BD Biosciences		1:200	
Cleaved Caspase-3 (Asp175)	Rabbit/ 5A1E	9664	Cell Signaling			1:100
Cleaved Notch1 (Val1744)	Rabbit/ D3B8	4147	Cell Signaling		1:100	1:100
E-cadherin	Mouse/ G-10	sc-8426	Santa Cruz		1:50	1:200
E-cadherin	Rabbit/ 24E10	3195	Cell Signaling	1:1000		
FRA1	Mouse/ C-12	sc-28310			1:50	1:50
GFP	Mouse/ 4B10	2955	Cell Signaling		1:100	
GFP	Rabbit	2555	Cell Signaling		1:100	
HES1	Rabbit/ D6P2U	11988	Cell Signaling	1:1000		1:50
Ki67	Mouse/ MIB-1	M7240	Agilent			1:150
Ki67	Rabbit/ D2H10	9027	Cell Signaling		1:100	
Laminin-5-γ2	Mouse/ D4B5	MAB19562	Merck Millipore		1:200	
Phospho p44/42 MAPK (Thr202/Tyr204)	Rabbit	9101	Cell Signaling	1:1000		
Tubulin	Mouse/ DM1A	T6199	Sigma-Aldrich	1:50000		
Vimentin	Mouse/ V9	M0725	Agilent			1:150

Immunoblotting (WB), immunofluorescence (IF), immunohistochemistry (IHC)

3.5.2 Secondary antibodies

Antibody	Species	Application	Supplier
Anti-Mouse AP Polymer	-	IHC	Zytomed Systems GmbH
Anti-Mouse Biotin	Goat	IF	Thermo Fisher Scientific Inc.
Anti-Mouse HRP	Goat	WB	Promega GmbH
Anti-Rabbit Biotin	Goat	IF	Thermo Fisher Scientific Inc.
Anti-Rabbit HRP	Goat	WB	Sigma-Aldrich

Immunoblotting (WB), immunofluorescence (IF), immunohistochemistry (IHC)

3.6 Buffers and solutions

4x Lower gel buffer

- 0.4 % SDS
- 1.5 M TRIS, pH 8.8

4x Upper gel buffer

- 0.4 % SDS
- 500 mM TRIS, pH 6.8

10x PCR buffer

- 100 mM β-Mercaptoethanol
- 67 mM $MgCl_2$
- 166 mM Ammonium sulphate
- 670 mM TRIS, pH 8.8

10x Running buffer

- 1.92 M Glycine
- 1 % SDS
- 250 TRIS, pH 8.5

10x TBS buffer

- 150 mM NaCl
- 20 mM TRIS, pH 7.6

1x TBST buffer

- 10x TBS buffer
- 0.1 % Tween 20

10x Transfer buffer

- 1.92 M Glycine
- 20 % Methanol
- 1 % SDS
- 250 mM TRIS, pH 8.5

50x TAE buffer

- 20 mM Acetic acid
- 1 mM EDTA
- 40 mM TRIS, pH 8.0

Annealing buffer

- 1 mM EDTA
- 50 mM NaCl
- 10 mM TRIS, pH 7.5- 8.0

AZD solvent

- Aqua ad iniectablia
- 0.5 % Methocel
- 0.2 % Tween 80

DBZ solvent

- Aqua ad iniectablia
- 0.5 % Methocel
- 0.1 % Tween 80

RIPA buffer

- 1 % NP 40
- 150 mM NaCl
- 0.1 % SDS
- 0.5 % Deoxycholic acid sodium salt
- 50 mM TRIS hydrochloride, pH 8.0

3.7 Laboratory equipment

Device	Supplier
Axioplan 2	Carl Zeiss GmbH, Oberkochen, Germany
BD FACSAria III	BD Bioscience, Heidelberg, Germany
BenchMark XT	Ventana Medical Systems, Inc., Tucson, AZ, USA
Centrifuge 5415R	Eppendorf AG, Hamburg, Germany
Heracell 240i CO_2 Incubator	Thermo Fisher Scientific Inc., Waltham, MA, USA
Heraeus Megafuge 40R Centrifuge	Thermo Fisher Scientific Inc., Waltham, MA, USA
Herasafe™ KSP Class II Biological Safety Cabinet	Thermo Fisher Scientific Inc., Waltham, MA, USA
HiSeq 1500	Illumina, Inc., San Diego, CA, USA
Image Station 440 CF	Kodak, Rochester, New York, USA
Liquid nitrogen cooled mortar	Bel-Art – SP Scienceware, Wayne, NJ, USA
LSM 700	Carl Zeiss GmbH, Oberkochen, Germany
Mini-PROTEAN Tetra Cell	Bio-Rad, Munich, Germany
MultiImage Light Cabinet	Alpha-InnoTec, Kasendorf, Germany
NanoDrop 1000 Spectrophotometer	Thermo Fisher Scientific Inc., Waltham, MA, USA
Pannoramic DESK II DW	3DHISTECH Ltd., Budapest, Hungary
PerfectBlue™ 'Semi-Dry'-Blotter, Sedec™	Peqlab Biotechnologie GmbH, Erlangen, Germany
peqPOWER	Peqlab Biotechnologie GmbH, Erlangen, Germany
PyroMark Q24 Advanced System	Qiagen GmbH, Hilden, Germany
T100™ Thermal Cycler	Bio-Rad, Munich, Germany
Theromixer comfort	Eppendorf AG, Hamburg, Germany
Varioskan Flash Multimode Reader	Thermo Fisher Scientific Inc., Waltham, MA, USA

4 METHODS

4.1 Cloning of pLenti Trace

All template plasmids were obtained from Addgene (www.addgene.org). For the Cre-sensitive recombination vector pLenti Trace, the previously described vector pLenti Multicolor [135] was used as template. Its expression cassette containing tagged-fluorescent color coding genes and Cre-recombinase recognition sides was replaced from Sma1 to Sal1 restriction sites by a synthetic sequence adding loxN sites as well as Nru1 and Pml1 restriction sites. Synthetic paired mCherry-FLAG (Integrated DNA Technologies, Inc.) then was inserted into the Nru1 site. The second tagged-fluorescent color EYFP-V5 was obtained by cleavage of pcDNA3.1 EYFP-V5 [135] with EcoR1 and Not1 restriction enzymes. To generate blunt ends, 5'-overhangs were filled in with Klenow Fragment. Finally, the coding gene of EYFP-V5 was inserted into the Pml1 restriction site yielding pLenti Trace. Modified vector elements were verified by restriction analysis and Sanger sequencing (GATC Biotech AG).

4.2 Bacterial cell culture

For cloning procedures and replication of plasmids carrying an ampicillin resistance, the *Escherichia coli* DH5α strain was used. The bacterial cells were cultured overnight at 37 °C in LB-medium supplemented with 100 µg/ml ampicillin to select for antibiotic-resistant clones. For bacterial transformation, plasmid DNA was added to competent *E. coli* DH5α and incubated for 30 minutes on ice. After a heat-shock for 45 seconds at 42 °C, the bacteria were placed on ice for two minutes and then incubated in 500 µL antibiotic-free LB medium for 45 minutes at 37 °C. Subsequently, the bacterial cells were plated on LB agar plates supplemented with ampicillin and then incubated overnight at 37 °C. To multiply transformed bacteria, LB medium

containing ampicillin was inoculated with a single bacterial colony followed by overnight incubation at 37 °C. Depending on the liquid culture volume, plasmid DNA was isolated using the mi-Plasmid Miniprep Kit (Metabion International AG) or the PureYield™ Plasmid Midiprep System (Promega GmbH) following the manufacturer's protocol.

4.3 Mammalian cell culture

4.3.1 Propagation of human cell lines and patient-derived colon cancers

HEK293 and SW480 cells were obtained from ATCC and SW1222 from the Ludwig Institute for Cancer Research (New York, USA). Cell lines were cultured in DMEM containing 10 % FBS, 100 U/ml penicillin and 0.1 mg/ml streptomycin (Biochrom). To establish patient-derived colon cancers, tissue samples of two human primary colorectal adenocarcinomas were provided by the biobank under administration of the foundation Human Tissue and Cell Research (HTCR) [138]. Patient-derived colon cancers were cultivated as spheroids in StemPro™ hESC SFM (Thermo Fisher Scientific Inc.) supplemented with 20 ng/ml EGF, 10 ng/ml FGF-basic (Thermo Fisher Scientific Inc.), 100 U/ml penicillin, and 0.1 mg/ml streptomycin (Biochrom) using ultra-low attachment cell culture flasks (Corning Life Sciences). All cells were kept in a humidified incubator at 37 °C and 5 % CO_2. For cryo-preservation, human cell lines and patient-derived colon cancers were slowly cooled to -80 °C in cryogenic tubes (neoLab Migge GmbH) using 90 % FBS and 10 % DMSO (Carl Roth GmbH) and Biofreeze freezing medium (Biochrom), respectively. For long-term storage, cells were transferred into liquid nitrogen.

4.3.2 Lentiviral transductions

For lentiviral transductions, HEK293 were co-transfected with 10 µg lentiviral vector, 10 µg pCMV-dR8.91 [136] and 3 µg pMD2.G [137] using LipoD293 (Tebu-bio) according to the manufacturer's protocol. Virus containing medium was passed through 0.45 µm

filters (Millipore), Lenti-X Concentrator (Clontech) was added and the mixture was incubated for 30 minutes at 4 °C. After centrifugation at 1,500 x g for 45 minutes at 4 °C, the pellet was resuspended in complete DMEM. The virus containing medium was used to infect SW480 colon cancer cells in the presence of 8 mg/mL polybrene (Sigma-Aldrich). pLenti rtTA3G (kind gift from Dominic Esposito), pLenti TetO-CreERT2 [135], and pLenti Trace triple transduced SW480 cells were selected with blasticidin (Carl Roth GmbH) and puromycin (Merck Millipore). Then cells were single cell sorted into 96-well plates on a FACSAria III instrument (BD Biosciences) and expanded. Recombination was tested *in vitro* by addition of 0.5 µg/ml doxycycline and 1 µM 4-hydroxytamoxifen (Sigma Aldrich), before xenotransplantation into mice.

4.4 Tumor xenografts and *in vivo* treatments

Mouse experiments were reviewed and approved by the Regierung von Oberbayern and mice were housed in pathogen free micro-isolator cages. Disaggregated primary colon cancers (PDX1 and PDX2), as well as SW1222 or SW480 colon cancer cells either native or carrying the lineage tracing constructs, were suspended in 200 µl of a 1:1 mixture of PBS and growth factor-depleted Matrigel (Corning Life Sciences). This mixture then was injected subcutaneously into age- and gender-matched 6-8 week old NOD/SCID mice (NOD.CB17-Prkdc^{scid}, The Jackson Laboratory) for xenograft formation. Mice were randomly assigned to control or treatment groups when tumor volumes reached 100 mm^3. For short term therapy and tracing experiments, mice were treated daily with 1.25 mg selumetinib (AZD6244, Selleckchem) *p.o.* or 0.35 mg dibenzazepine (DBZ, Axon Medchem BV) *i.p.* for 5 days. For lineage tracing, 2.5 µg doxycycline were given *p.o.* for 2 days starting on day 3, and recombination of pLenti Trace was induced by 7.5 ng tamoxifen *i.p.* (Sigma Aldrich). For BrdU tracing, mice were injected with 1.25 mg BrdU (Sigma Aldrich) 18 hours after last inhibitor treatment. For long-term therapy, mice were treated with 1.25 mg AZD and 0.35 mg DBZ, or vehicle as control, every 3 days until tumors reached volumes of

1,000 –1,300 mm^3. Mice were sacrificed, tumors removed, and either formalin fixed and paraffin embedded for histology and immunostaining, or directly used for gene expression analysis and immunoblotting.

4.5 Immunoblotting

For immunoblotting, freshly harvested and snap-frozen tumor samples were ground in a liquid nitrogen-cooled mortar (Bel-Art). 60 mg of tissue powder was lysed in RIPA buffer supplemented with protease and phosphatase inhibitors (Roche Diagnostics GmbH). Samples then were sonicated for 20 seconds, incubated for 30 minutes at room temperature and centrifuged at 35,000 x g for another 30 minutes. Protein concentrations of the supernatants were measured with the DC Protein Assay (Biorad) according to the manufacturer's protocol using a Varioskan Flash Multimode Reader (Thermo Fisher Scientific Inc.). For protein denaturation, 4x Laemmli sample buffer (Biorad) was added to 30 µg protein sample and heated for five minutes at 95 °C. Then samples were loaded on a 10 % SDS polyacrylamide gel and separated by electrophoresis at 90-170 V using a Mini-PROTEAN Tetra Cell (Biorad) filled with TRIS-glycine-SDS running buffer. Subsequently, proteins were transferred onto Immobilon-P PVDF membranes (Merck Millipore) using transfer buffer and the PerfectBlue™ 'Semi-Dry'-Blotter, Sedec™ (Peqlab) kept constantly at 100 mA per gel. To avoid non-specific antibody binding, membranes were blocked in 5 % skim milk/1x TBST for 60 minutes, followed by overnight incubation at 4 °C with primary antibodies dissolved in 5 % BSA (Carl Roth GmbH) and 1x TBST. For visualization of protein bands, membranes were incubated in horseradish peroxidase (HRP)-conjugated secondary mouse (Promega GmbH) or rabbit (Sigma-Aldrich) antibodies. Subsequently, a chemiluminescent HRP substrate (Merck Millipore) was added and signals were detected using an Image Station 440 CF (Kodak). Primary and secondary antibodies used are listed in section 3.5.1 and 3.5.2, respectively.

4.6 Histological staining procedures

4.6.1 Immunohistochemistry

For immunohistochemistry, 5 µM tissue sections of CRC samples or xenografts were deparaffinized and stained on a BenchMark XT autostainer (Ventana Medical Systems, Inc.) using primary antibodies as listed in section 3.5.1. Staining was visualized with ultraView or optiView DAB detection kits (Ventana Medical Systems, Inc.). Immunohistochemical detection of cleaved Caspase-3 and Vimentin was performed manually on deparaffinized sections by retrieving antigens in citrate (Agilent) for 20 min in a microwave oven followed by incubation with primary antibodies. For visualization of cleaved Caspase-3, the ImmPRESS™ HRP Anti-Rabbit IgG Polymer Detection Kit (Vector Laboratories Inc.) and the liquid DAB+ Substrate Chromogen System (Agilent) were used according to the manufacturer's protocols. Immunostainings of Vimentin were visualized by incubation with alkaline phosphatase (AP)-coupled secondary antibodies and AP substrate kits (Zytomed Systems GmbH). Primary and secondary antibodies are provided in section 3.5.1 and 3.5.2, respectively. The intratumoral distribution of NICD and HES1 staining was determined by inspection of tumor edge and tumor center in each case. For survival analysis, NICD-positive tumor cells were scored in 10 % steps by estimation. FRA1 expression was scored semi-quantitatively, ranging from complete absence (score 0), weak (score 1), moderate (score 2), or strong expression (score 3). Cases then were classified as FRA1 negative (score 0) and FRA1 positive (scores 1-3). Immunostainings of xenografts were analyzed by counting positive tumor cells or by quantification of staining intensities using ImageJ software (NIH).

4.6.2 Immunofluorescence

For double immunofluorescence, a semi-automated protocol was established to intensify the staining of weakly detectable proteins. 5 µM tissue sections were deparaffinized and stained for primary antibodies on a BenchMark XT autostainer (Ventana Medical Systems, Inc.). For signal amplification and visualization, Cyanine 3-conjugated tyramide (Perkin Elmer) was used as HRP substrate and applied manually. Tissue sections then were incubated in additional primary antibodies followed by signal amplification using biotin-labeled secondary mouse or rabbit antibodies. Streptavidin-conjugated Alexa Fluor 488 was used for visualization and nuclei were counterstained with DAPI (Carl Roth GmbH). Primary and secondary antibodies are given in section 3.5.1 and 3.5.2, respectively. A LSM 700 laser scanning microscope (Carl Zeiss GmbH) and the ZEN software (Carl Zeiss GmbH) were used for taking confocal fluorescence images. Contrast and brightness were adjusted in Adobe Photoshop, and for NICD staining a nuclear mask was applied. Co-localization of fluorescence signals was quantified using Volocity 6.1.1 software (Perkin Elmer) and plotted as percentage values of maximum fluorescence intensity.

4.7 Gene expression analysis and GSEA

For RNA isolation, 50 mg of freshly ground tumor samples was further homogenized in QIAzol lysis reagent (Qiagen GmbH). Libraries were constructed using the mRNA Sense library preparation kit (Lexogen GmbH) according to manufacturer's protocol. In brief, 500 ng of total RNA was captured on oligo dT beads, hybridized to random primers and stoppers for cDNA synthesis and ligated. Single stranded cDNAs with sequencing adapters then were amplified and barcoded, and libraries were purified with AMPure XP beads (Beckman Coulter GmbH), quantified, pooled at 10 nM concentration, and sequenced in multiplex on a HiSeq 1500 (Illumina, Inc.) as 50 bp single reads. Subsequently, data were demultiplexed, adaptor sequences were

removed and the reads were mapped to the hg19 human reference genome. Sequence reads for annotated genes were counted with the HTseq count script from the DEseq2 package and differentially expressed genes were identified with the edgeR package with a <1 % false discovery rate (FDR). Heat maps and clustering were done with GENE-E (Broad Institute). Hallmark gene sets [139] most enriched in each cluster were determined using Gene Set Enrichment Analysis (GSEA) software [140]. For enrichment curves, GSEA analyses were run with 1000 permutations. RNA-seq expression data are accessible through GEO (GSE98922).

4.8 Clinical samples

CRC specimens from patients that underwent surgical resection at the University of Munich between 1994 and 2007 (LMU; Munich) were obtained from the archives of the Institute of Pathology. The Munich Cancer Registry recorded the follow-up data prospectively. Specimens were anonymized, and the study was approved by the institutional ethics committee of the Medical Faculty of the LMU. For the UICC stage II collection, inclusion criteria were colorectal adenocarcinomas with bowel wall infiltration (T3, T4) but absence of nodal (N0) or distant metastasis (M0) at the time of diagnosis. The final collection consisted of 225 cases with 50 events of cancer-specific death and 71 events of tumor progression, either documented as tumor recurrence or metastasis. For the metastasis collection, a case control design was selected, including tumor specimens of 92 patients. Half of the patients had colon cancers with synchronous liver metastasis (UICC stage IV), diagnosed by clinical imaging or liver biopsy. Colon cancer patients without distant metastasis at the time of diagnosis (UICC stages I-III) and with five year disease-free survival after primary surgical resection were applied as controls. Cases and controls were matched by tumor grade (according to WHO 2010), T-category, and tumor location (all tumors were right-sided colon cancers), resulting in 46 matched pairs.

Furthermore, 11 paired tissue samples of primary colorectal cancers and their metastases to different sites were collected. For *KRAS* mutational testing, tumor tissue was scraped from deparaffinized tissue sections under microscopic control using sterile scalpel blades. Tumor DNA was extracted with the QIAamp DNA Micro Kits (Qiagen GmbH) following the manufacturer's protocol. *KRAS* exon 2 then was PCR amplified using the primers KRAS fwd and KRAS rev, and HotStar Taq DNA Polymerase (Qiagen GmbH). Subsequently, *KRAS* exon 2 was analyzed by pyrosequencing on the PyroMark Q24 Advanced System (Qiagen) with the primers KRAS fwd and KRAS exon 2 rev. Primer sequences are provided in section 3.4.1.

4.9 Statistical analysis

Two-tailed Student's t test was used to evaluate significant differences between two groups, and data indicate means ± SD, unless indicated otherwise. For patient outcome and mouse survival, the Kaplan-Meier method was used and *P*-values were calculated by the log-rank test. Cox proportional hazards model was used for multivariate analysis. Differences were considered statistically significant when $P < 0.05$. Individual *P*-values are given within the figures. Statistics were calculated with GraphPad Prism (GraphPad software, Inc.) or SPSS (IBM).

5 RESULTS

5.1 High NOTCH activity indicates a distinct tumor cell subpopulation in colon cancer

To obtain insights into the role of the NOTCH pathway in CRC, we examined tissue specimens of a total of 328 adenocarcinomas for accumulation of NICD, which indicates activation of NOTCH signaling. Immunostaining revealed widespread nuclear accumulation of NICD in tumor cells of most cases (80.5 %; Figure 6).

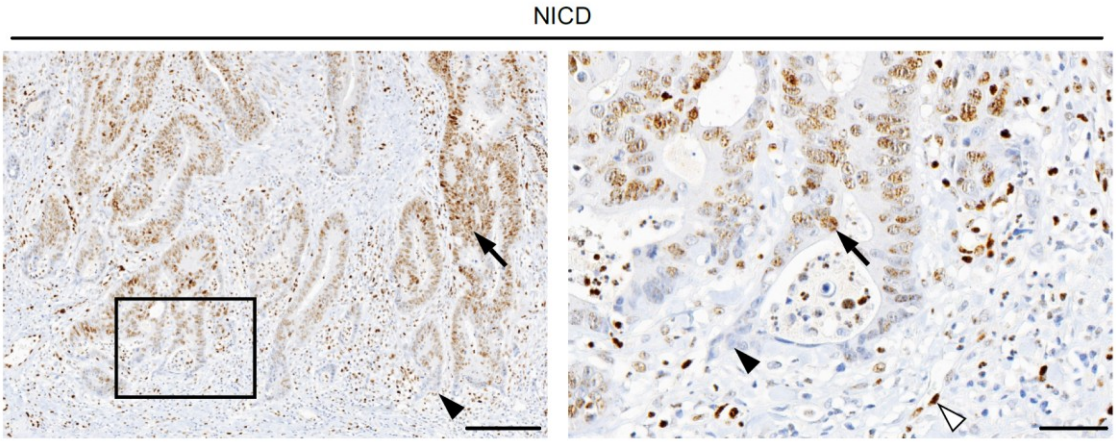

Figure 6. Distribution of colorectal cancer cells with high NOTCH activity.

Representative immunostaining for NICD in primary colon cancer tissue. Right panel shows higher magnification of area boxed in the left panel. Arrowheads indicate tumor cells at the tumor edge, and arrows indicate tumor cells toward the tumor center; open arrowhead indicates an endothelial cell. Scale bars: 200 µm (left); 20 µm (right).

Interestingly, however, NICD was not evenly distributed within these tumors. Specifically, colon cancer cells that were located at the tumor edge were negative for NICD in 89.4 % of these cases, whereas, in contrast, tumor cells located closer to the tumor center abruptly became NICD positive (Figure 6). We then examined the NOTCH effector HES1 in a subset of 225 cases. Similar to the pattern of NICD, we also found expression in the center of colorectal cancers (66.2 %), whereas its expression was diminished or absent in tumor cells at the tumor edge (Figure 7).

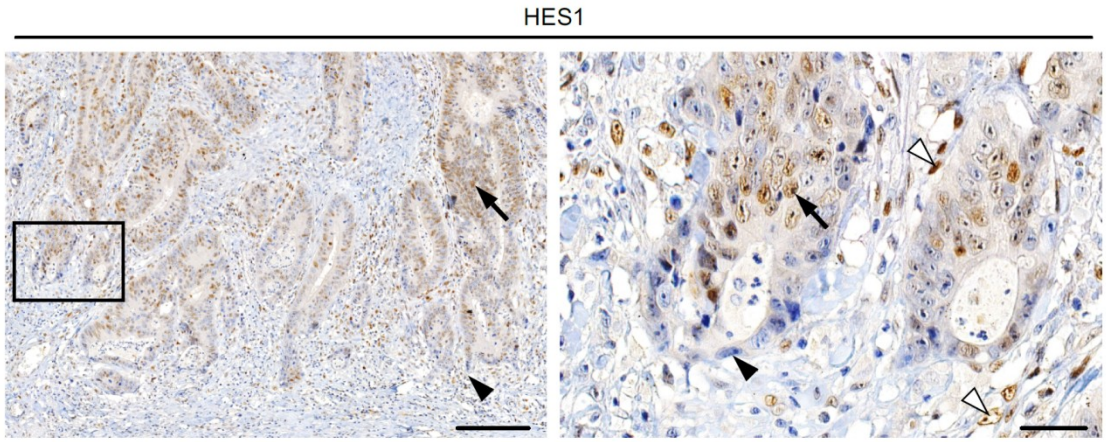

Figure 7. Distribution of HES1 expression in colorectal cancer.

Representative immunostaining for HES1 in primary colon cancer tissue. Right panel shows higher magnification of area boxed in the left panel. Arrowheads indicate tumor cells at the leading tumor edge, and arrows indicate tumor cells toward the tumor center; open arrowheads indicate endothelial cells. Scale bars: 200 µm (left); 20 µm (right).

Collectively, these findings showed that NOTCH signaling is activated in the center of colorectal cancers but unexpectedly downregulated at the infiltrative tumor edge.

Colon cancer cells at the tumor edge are known to activate MAPK and WNT signaling [26]. Therefore, we compared the activity of both pathways with the status of the NOTCH pathway. Using FRA1 and nuclear β-catenin as indicators for MAPK and WNT activity, respectively, we found that tumor cells with strong staining for these markers showed significantly decreased or absent staining for NICD (Figure 8, A-D).

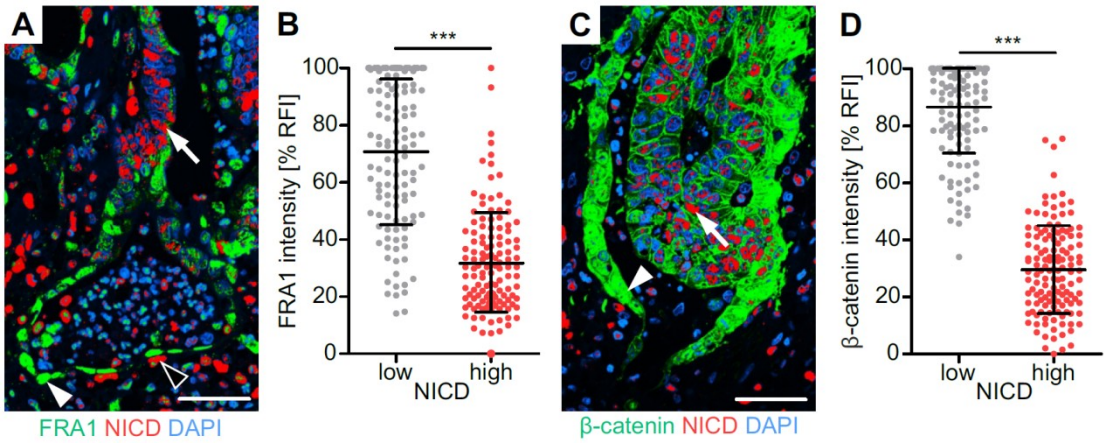

Figure 8. Comparison of active MAPK and WNT signaling with high NOTCH activity in colorectal cancer cells.

(A and C) Double immunofluorescence for indicated proteins in representative colon cancer tissues. Arrowheads indicate tumor cells at the tumor edge, and arrows indicate tumor cells toward the tumor center. Open arrow indicates endothelial cells at the tumor edge. Scale bars, 50 µM. **(B and D)** Quantification of co–immune fluorescence signals. Relative fluorescence intensities (% RFI) for indicated proteins in tumor cells with high (upper quartile) and low (lower quartile) NICD staining intensity are shown. Data are derived from n ≥ 500 tumor cells in n = 10 different CRC cases. Error bars indicate mean ± SD. ***, $P < 0.001$ by t test.

On the contrary, colon cancer cells with high levels of NICD showed much lower expression of FRA1 and nuclear β-catenin (Figure 8, A-D). Moreover, tumor cells that were positive for NICD on average were more numerous than FRA1-positive tumor cells (Figure 9 A). Additionally, NICD-positive tumor cells showed higher proliferation rates than tumor cells with FRA1 expression (Figure 9 B).

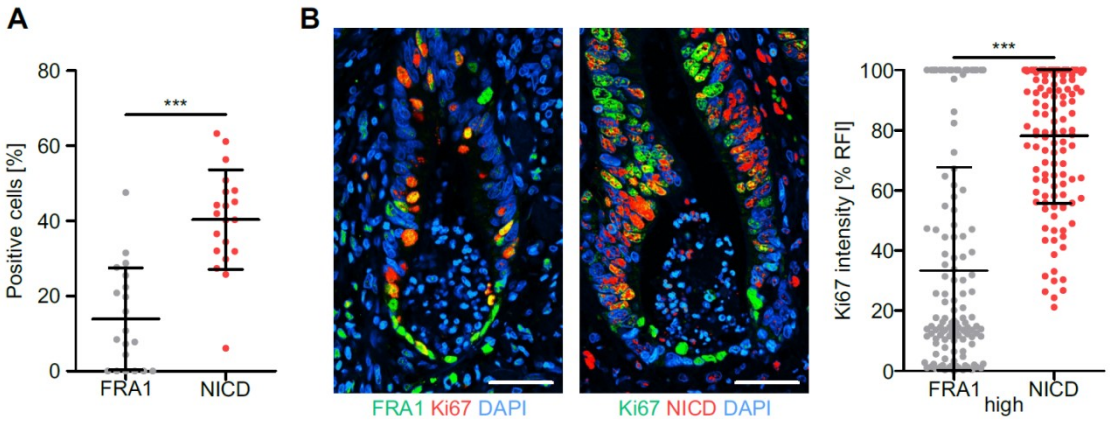

Figure 9. Characteristics of FRA1- and NICD-positive tumor cells in colorectal cancer.

(A) Quantification of FRA1- and NICD-positive tumor cells in n = 20 different primary colon cancers. **(B)** Double immunofluorescence (left panels) and quantification of co-immune fluorescence signals (right panel) for Ki67 and FRA1 or NICD. Relative fluorescence intensities (% RFI) for Ki67 in individual tumor cells with high (upper quartile) FRA1 and NICD staining intensity are shown. Data are derived from n ≥ 500 tumor cells in n = 10 different CRC cases. Error bars indicate mean ± SD. ***, $P < 0.001$ by t test. Scale bars, 50 µm.

High activities of NOTCH and MAPK/WNT therefore were mutually exclusive in colon cancer cells and marked distinct tumor cell subpopulations. Next, we tested for an association of NOTCH signaling and EMT. Double immunofluorescence staining showed that colon cancer cells with high LAMC2 expression levels, a marker indicating EMT in colon cancer [90], were devoid of strong NICD accumulation, whereas, in contrast, colon cancer cells with high NICD levels showed low LAMC2 expression (Figure 10, A and B).

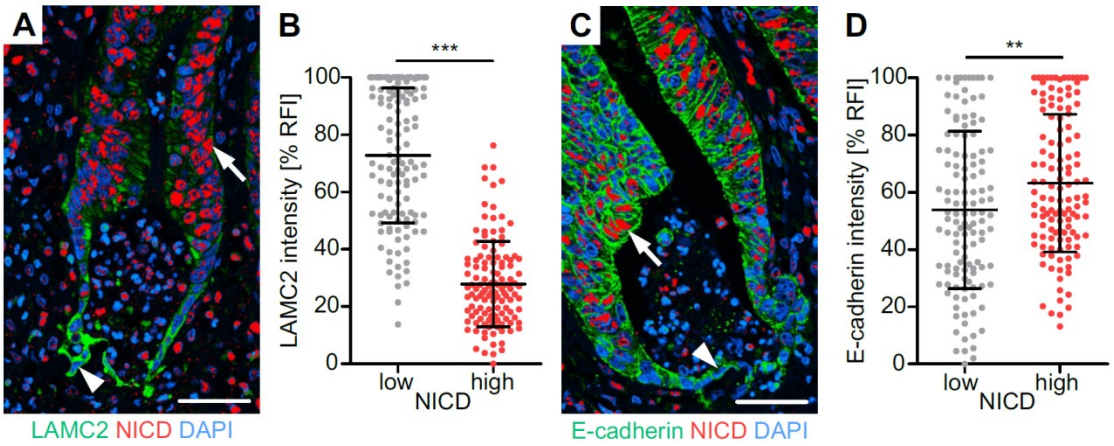

Figure 10. Association of NOTCH signaling and EMT phenotype.

(A and C) Double immunofluorescence for indicated proteins in representative colon cancer tissues. Arrowheads indicate tumor cells at the tumor edge, and arrows indicate tumor cells toward the tumor center. Scale bars, 50 µM. **(B and D)** Quantification of co–immune fluorescence signals. Relative fluorescence intensities (% RFI) for indicated proteins in tumor cells with high (upper quartile) and low (lower quartile) NICD staining intensity are shown. Data are derived from n ≥ 500 tumor cells in n = 10 different CRC cases. Error bars indicate mean ± SD. **, $P < 0.01$;***, $P < 0.001$ by t test.

Moreover, colon cancer cells with high NICD levels had significantly higher expression of the epithelial cell adhesion molecule E-cadherin, when compared with colon cancer cells with low NICD levels (Figure 10, C and D). These findings demonstrate that colon cancers are composed of distinct tumor cell subpopulations, including tumor cells at the tumor edge with high MAPK and WNT activity undergoing EMT and tumor cells with high NOTCH activity in the tumor center that have a more epithelial phenotype.

5.2 MAPK and NOTCH activity are associated with colon cancer progression

Next, we investigated the clinical relevance of tumor cell subpopulations with high MAPK and NOTCH activity by scoring FRA1 and NICD in our collection of CRC cases (Figure 11). 225 of these cases were UICC stage II colorectal cancers with recorded clinical follow-up data (Table 1).

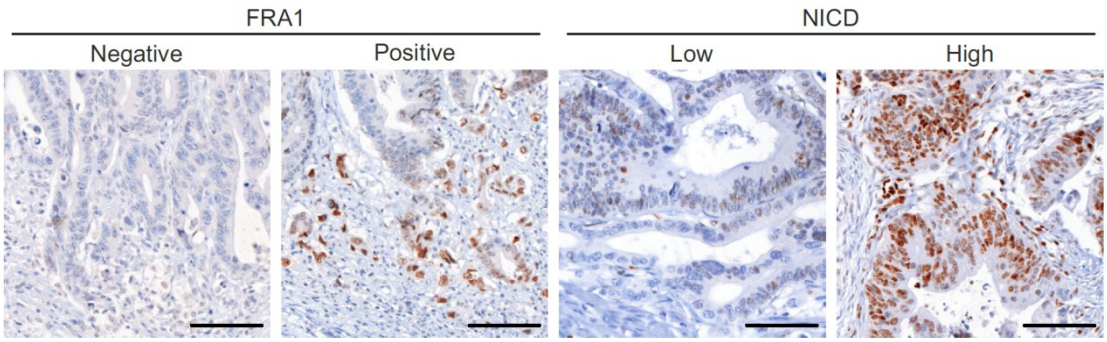

Figure 11. Scoring of FRA1 and NICD in colorectal cancer.

Assessment of FRA1 and NICD in primary human colorectal cancers. For FRA1, tumors were categorized as negative or positive, based on absence or presence of detectable immunostaining in tumor cells. For NICD, cases were categorized as low or high, based on less or more than 10 % tumor cells with strong NICD staining, respectively. Scale bars, 50 µm.

Table 1. Clinical data of FRA1 and NICD expression in UICC stage II colorectal cancer.

Characteristics	Total	FRA1			NICD			FRA1/NICD combination		
		negative	positive	*P*	low	high	*P*	negative/low	others	*P*
All patients	225	53 (23.6)	172 (76.4)		51 (22.7)	174 (77.3)		20 (8.9)	205 (91.1)	
Age (y, Median 69)										
≤ 68	112	29 (25.9)	83 (74.1)	0.411	24 (21.4)	88 (78.6)	0.659	10 (8.9)	102 (91.1)	0.983
≥ 69	113	24 (21.2)	89 (78.8)		27 (23.9)	86 (76.1)		10 (8.8)	103 (91.2)	
Gender										
Male	121	33 (27.3)	88 (72.7)	0.156	27 (22.3)	94 (77.7)	0.892	11 (9.1)	110 (90.9)	0.909
Female	104	20 (19.2)	84 (80.8)		24 (23.1)	80 (76.9)		9 (8.7)	95 (91.3)	
T-stage (UICC)										
T3	186	41 (22.0)	145 (78.0)	0.243	43 (23.1)	143 (76.9)	0.724	16 (8.6)	170 (91.4)	0.741
T4	39	12 (30.8)	27 (69.2)		8 (20.5)	31 (79.5)		4 (10.3)	35 (89.7)	
Tumor grade (WHO)										
low grade	201	42 (20.9)	159 (79.1)	0.007	40 (19.9)	161 (80.1)	0.004	13 (6.5)	188 (93.5)	<0.001
high grade	24	11 (45.8)	13 (54.2)		11 (45.8)	13 (54.2)		7 (29.2)	17 (70.8)	
KRAS Exon 2										
wild-type	139	38 (27.3)	101 (72.7)	0.089	34 (24.5)	105 (75.5)	0.414	14 (10.1)	125 (89.9)	0.428
mutated	86	15 (17.4)	71 (82.6)		17 (19.8)	69 (80.2)		6 (7.0)	80 (93.0)	

Row percent values are given in parentheses. *P*-values indicate Chi-square test results

Kaplan-Meier statistics revealed that FRA1-negative cases were associated with a tendency toward better cancer-specific and disease-free survival when compared with FRA1-positive cases (Figure 12).

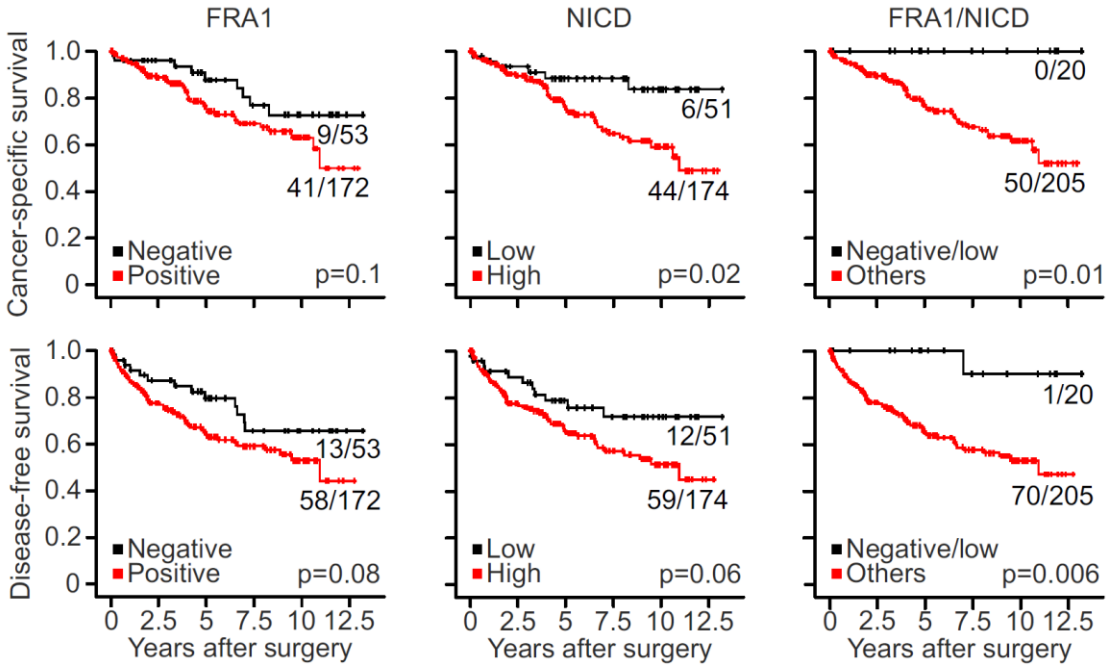

Figure 12. Survival analyses of FRA1, NICD, and their combination in colorectal cancer.

Survival associations of FRA1, NICD, and their combination in 225 UICC stage II colorectal cancers. Kaplan-Meier plots for cancer-specific survival and disease-free survival are shown. *P*-values are log-rank test results. Ratios on curves indicate the number of events over the number of patients per group.

We then tested for associations with NICD staining and found that colorectal cancers with <10 % NICD-positive tumor cells (NICD low) also showed significantly better cancer-specific and disease-free survival than cases with higher frequencies of NICD-positive tumor cells (NICD high; Figure 12). Furthermore, when testing a combined evaluation of FRA1 and NICD, we found that patients whose tumors were both FRA1 negative and NICD low almost perfectly survived the follow-up period, with no event of cancer-specific death and only one event of tumor progression (Figure 12). In contrast, patients whose tumors were either FRA1 positive, NICD high, or both showed significantly poorer cancer-specific and disease-free survival. Testing for associations with other clinical and pathological variables revealed that FRA1 positivity and high NICD levels were more frequent in low than in high-grade colon cancers, whereas the other core clinical variables T-category, age, and sex, as well

as KRAS mutation status were not linked to FRA1 or NICD (Table 1). We then included these variables into proportional hazards regression analyses and found that combined absence of FRA1 and NICD was an independent predictor of favorable outcome for disease-free survival (Table 2).

Table 2. Multivariate analysis of disease-free survival in UICC stage II colorectal cancer.

Variables	Disease free survival		
	HR	(95% confidence interval)	*P*
Age (≥ vs < median)	1.0	(0.64-1.66)	0.902
Gender (F vs M)	1.0	(0.63-1.64)	0.938
T-stage	2.9	(1.73-4.82)	<0.001
Tumor grade	0.8	(0.32-2.03)	0.642
KRAS Exon 2 (mutated vs. wild-type)	1.3	(0.78-2.04)	0.348
FRA1/NICD combination (others vs negative/low)	9.9	(1.35-72.74)	0.024

Furthermore, we evaluated 92 colon cancers of a case-control collection of matched tumor pairs, with and without synchronous liver metastasis, applying the same scoring method as for the UICC II collection (Table 3).

Table 3. Clinical data of FRA1 and NICD expression in a case-control collection of colon cancers with and without distant metastasis.

Characteristics	Total	FRA1			NICD			FRA1/NICD combination		
		negative	positive	*P*	low	high	*P*	negative/low	others	*P*
All patients	92	22 (23.9)	70 (76.1)		13 (14.1)	79 (85.9)		5 (5.4)	87 (94.6)	
Age (y, Median 68)										
≤ 68	48	12 (25.0)	36 (75.0)	0.799	7 (14.6)	41 (85.4)	0.896	4 (8.3)	44 (91.7)	0.200
≥ 69	44	10 (22.7)	34 (77.3)		6 (13.6)	38 (86.4)		1 (2.3)	43 (97.7)	
Gender										
Male	45	11 (24.4)	34 (75.6)	0.907	6 (13.3)	39 (86.7)	0.830	2 (4.4)	43 (95.6)	0.682
Female	47	11 (23.4)	36 (76.6)		7 (14.9)	40 (85.1)		3 (6.4)	44 (93.6)	
T-stage (UICC)										
T2	8	1 (12.5)	7 (87.5)	0.369	1 (12.5)	7 (87.5)	0.640	1 (12.5)	7 (87.5)	0.437
T3	69	19 (27.5)	50 (72.5)		11 (15.9)	58 (84.1)		4 (5.8)	65 (94.2)	
T4	15	2 (13.3)	13 (86.7)		1 (6.7)	14 (93.3)		0 (0.0)	15 (100.0)	
Nodal status										
N0	39	14 (35.9)	25 (64.1)	0.021	8 (20.5)	31 (79.5)	0.132	4 (10.3)	35 (89.7)	0.080
N+	53	8 (15.1)	45 (84.9)		5 (9.4)	48 (90.6)		1 (1.9)	52 (98.1)	
Metastasis (Liver)										
M0	46	17 (37.0)	29 (63.0)	0.003	10 (21.7)	36 (78.3)	0.036	5 (10.9)	41 (89.1)	0.021
M1	46	5 (10.9)	41 (89.1)		3 (6.5)	43 (93.5)		0 (0.0)	46 (100.0)	
Tumor grade (WHO)										
low grade	30	6 (20.0)	24 (80.0)	0.540	2 (6.7)	28 (93.3)	0.153	1 (3.3)	29 (96.7)	0.536
high grade	62	16 (25.8)	46 (74.2)		11 (17.7)	51 (82.3)		4 (6.5)	58 (93.5)	

Row percent values are given in parentheses. *P*-values indicate Chi-square test results

We observed that tumors with liver metastases were significantly more often FRA1 positive, NICD high, or both, whereas on the contrary, none of the few tumors that were FRA1 negative and NICD low had metastasized (Figure 13; Table 3).

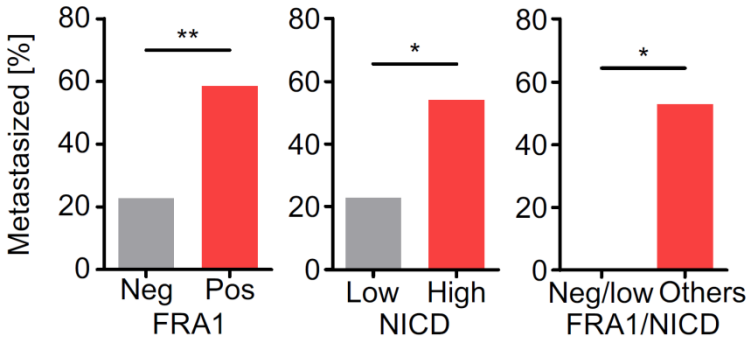

Figure 13. Association of FRA1, NICD, and their combination with metastasis in colorectal cancer.

Association of FRA1, NICD, and their combination with liver metastasis in a matched case-control collection of 92 colon cancers. *, $P < 0.05$; **, $P < 0.01$ by χ^2 test.

We then also examined another 11 colorectal cancers of which we obtained paired tissues of primary tumors and corresponding metastases to the liver (n = 6), the peritoneum (n = 3), or the lung (n = 2). Interestingly, nine metastases had recapitulated the patterns of FRA1- and NICD-positive tumor cells of their primary tumors, whereas only two, in contrast to their primary tumors, showed absent or lower FRA1 or NICD staining, respectively (Figure 14).

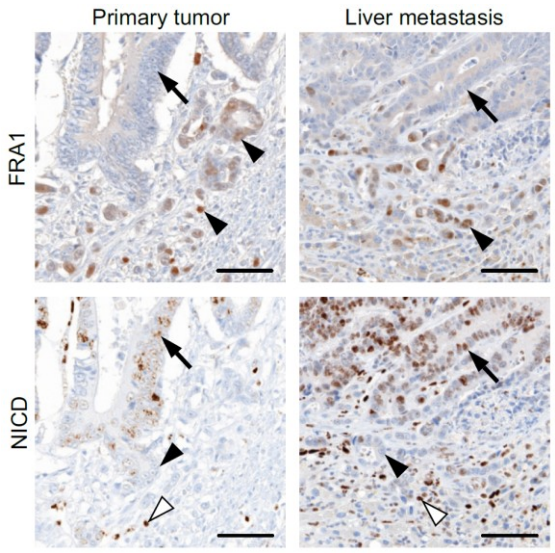

Figure 14. Distribution of FRA1 and NICD in colon cancer and corresponding liver metastasis.

Representative staining for FRA1 and NICD in a primary colon cancer and corresponding liver metastasis. Arrowheads indicate tumor cells at the tumor edge, and arrows indicate tumor cells toward the tumor center; open arrowheads indicate endothelial cells. Scale bars, 50 µm.

Collectively, these findings suggested that tumor cell subpopulations with MAPK and NOTCH activity are both important for colon cancer progression in early- and late-stage disease, frequently show similar presence in primary tumors and corresponding metastases, and that best clinical outcome may be expected if the activity of both pathways is low.

5.3 Colon cancers evade MAPK- or NOTCH-targeted therapy by shifting their phenotype

MAPK and NOTCH signaling can be repressed with the MEK inhibitor selumetinib (AZD) and the γ-secretase inhibitor dibenzazepine (DBZ), respectively. To evaluate the effects of either treatment, we used mouse models of cell line-derived SW480 or patient-derived PDX1 colon cancer xenografts (Figure 15).

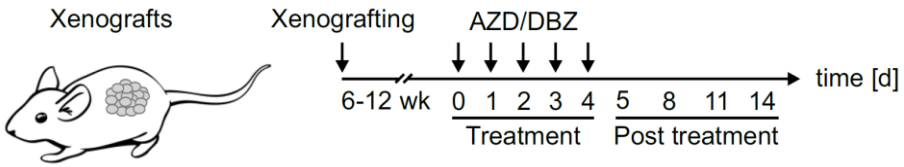

Figure 15. Experimental setup.
Schema and experimental schedule for xenografting, inhibitor treatment, and tumor analysis.

Xenograft tumors were composed of tumor cell subpopulations with strong expression of FRA1 at the tumor edge, and accumulation of NICD toward the tumor center and thus adequately modeled the intratumoral composition and distribution of MAPK and NOTCH activity in primary colon cancers (Figure 16 A).

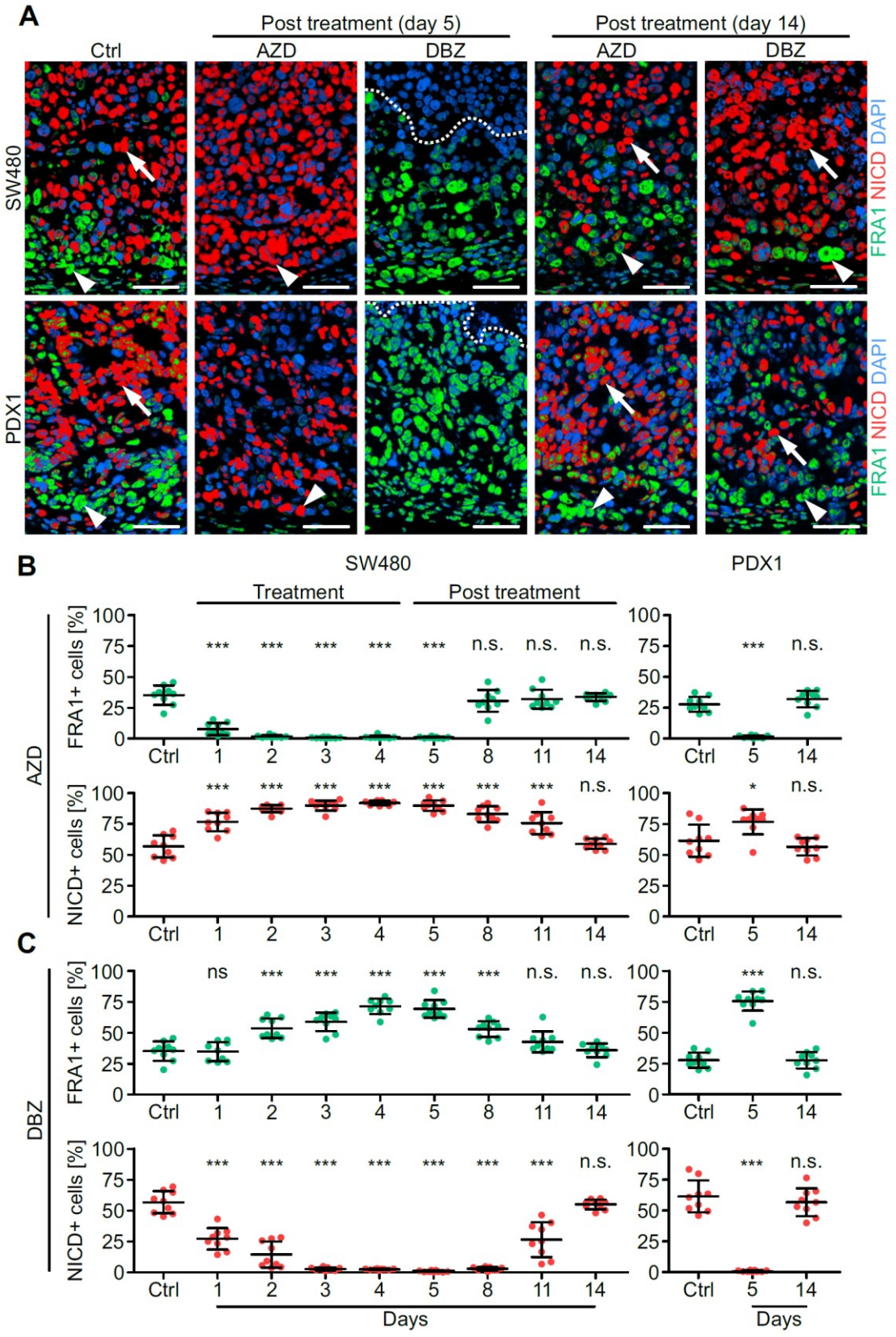

Figure 16. Effects of MAPK and NOTCH repression in colon cancer xenografts.

(A) Immunofluorescence for FRA1 and NICD in SW480 and patient-derived (PDX1) xenografts. Vehicle-treated tumors (Ctrl) and AZD- or DBZ-treated tumors at indicated time points were analyzed. Arrowheads indicate tumor cells at the tumor edge, and arrows indicate tumor cells toward the tumor center. Areas above dotted lines are tumor necrosis. Scale bars, 50 μm. **(B and C)** Quantification of FRA1- and NICD-positive tumor cells in SW480 and PDX1 xenografts. Vehicle-treated tumors (Ctrl) and tumors at indicated time points during and after AZD (B) or DBZ (C) treatment were analyzed. Error bars are mean ± SD. *, $P < 0.05$; ***, $P < 0.001$ by t test; n.s., not significant; compared with Ctrl. n ≥ 3 independent biological replicates.

We then treated mice bearing these xenografts with AZD for 5 d and observed that FRA1 expression was completely lost in these tumors (Figure 16, A and B). Time course analysis showed that in SW480 xenografts this already occurred after 2 d of treatment (Figure 16 B), which indicated strong and rapid repressive effects of AZD on MAPK signaling, as expected. Surprisingly, however, the frequency of NICD-positive tumor cells significantly expanded under AZD treatment in SW480 and PDX1 xenografts, and these cells then directly reached the tumor edge, suggesting an expansion of intratumoral NOTCH activity under MAPK repression (Figure 16, A and B). In addition, AZD treatment reduced the number of cleaved Caspase-3-labeled tumor cells, indicating that the loss of FRA1-positive tumor cells was not a result of increased apoptosis (Figure 17, A and B).

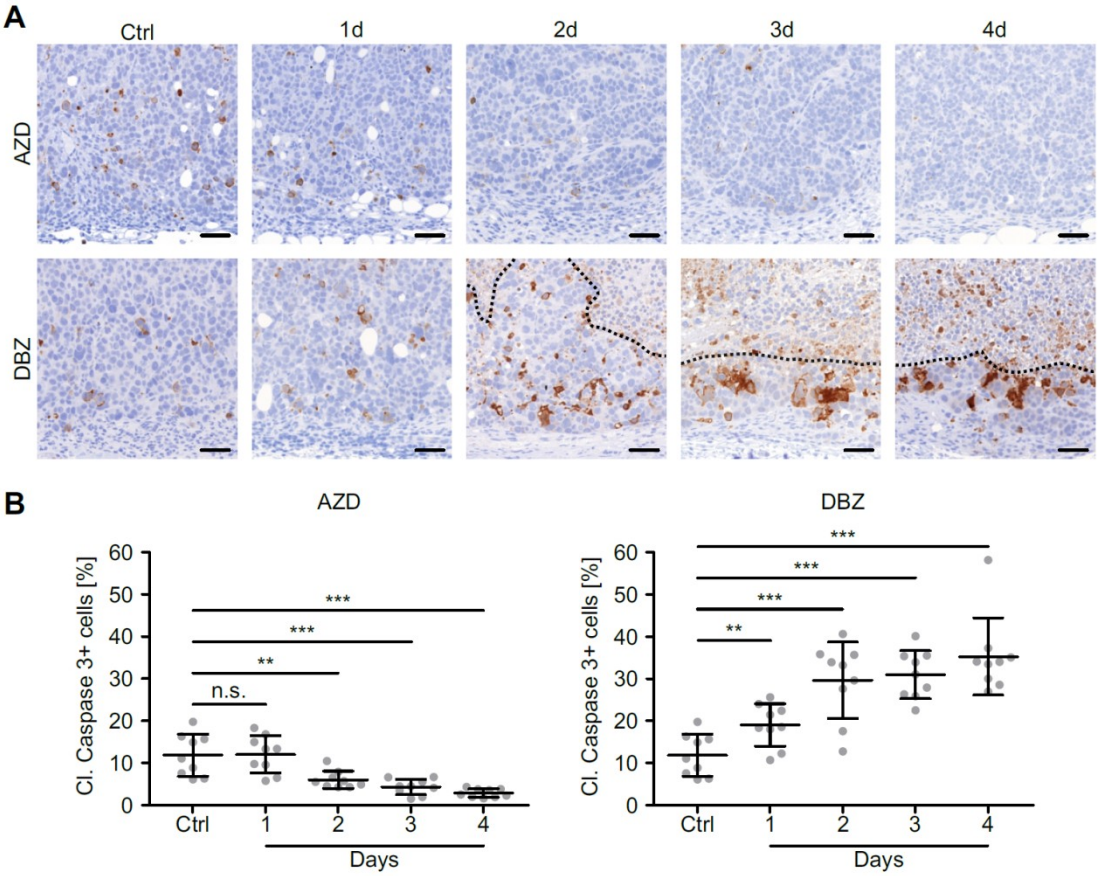

Figure 17. Effects of short-term AZD and DBZ treatment on apoptosis in colon cancer xenografts.

(A and B) Representative immunostainings (A) and quantification (B) of cleaved (Cl.) Caspase-3 in SW480 xenografts. Vehicle-treated tumors (Ctrl) and AZD- or DBZ-treated tumors at indicated time points were analyzed. Areas above dotted lines are tumor necrosis. Scale bars, 50 µm. Error bars are mean ± SD. **, $P < 0.01$; ***, $P < 0.001$ by t test; n.s., not significant. n ≥ 3 independent biological replicates.

These findings suggest that colon cancer cell subpopulations switched from MAPK to NOTCH activity upon MAPK repression. Next, to repress NOTCH signaling, we treated SW480 and PDX1 xenografts with DBZ and found complete depletion of NICD accumulation in these tumors that in time course analysis in SW480 xenografts was fully effective after 3 d of treatment (Figure 16, A and C). However, under DBZ treatment, the frequency of FRA1-positive tumor cells significantly increased, indicating expanded MAPK signaling upon repression of NOTCH activity (Figure 16, A and C). Furthermore, in contrast to MAPK inhibition, DBZ treatment significantly increased the number of cleaved Caspase-3-labeled tumor cells (Figure 17, A and B), suggesting that colon cancer cells with high NOTCH activity were at least in part lost from the tumor through apoptosis.

With these findings in mind, we then analyzed xenograft tumors of mice that had been treated with AZD or DBZ and subsequently had been taken off treatment for up to 10 d before analysis. Astonishingly, in these tumors the original distributions and frequencies of colon cancer cells with FRA1 expression at the tumor edge and NICD accumulation in more centrally located tumor cells were readily restored (Figure 16, A-C). Time course analysis in SW480 xenografts further demonstrated a quicker recovery of FRA1-positive tumor cells than of NICD-positive tumor cells from respective treatments (Figure 16, B and C). Collectively, these data indicated that colon cancers may evade targeted treatment against MAPK or NOTCH signaling by a reversible shift in predominating pathway activity.

5.4 MAPK and NOTCH have opposite effects on epithelial differentiation in colon cancer

To shed more light on the effects of therapeutic targeting of MAPK and NOTCH signaling in colon cancer, we analyzed gene expression in SW480 xenografts after AZD or DBZ treatment by RNA-Seq. Considering genes with at least twofold change in expression, we found that AZD treatment affected 12.1 % (2,822 genes) of the detected transcriptome, whereas DBZ treatment only deregulated 1.9 % (448 genes). Differentially expressed genes only partially overlapped, indicating discriminative effects of both treatments (Figure 18).

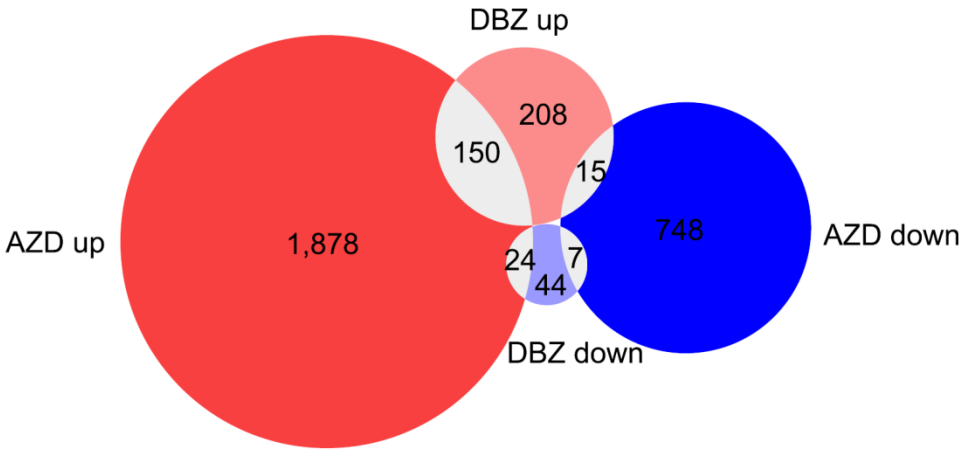

Figure 18. Differential gene expression after AZD and DBZ treatment.

Venn diagram of genes with significantly ($P < 0.05$) differential expression and two or more fold change in SW480 xenografts that were treated for five consecutive days with AZD or DBZ compared with vehicle treatment (Ctrl). n = 3 independent biological replicates.

Unsupervised hierarchical clustering of gene expression then revealed four major clusters that were characterized by repression (cluster A) or upregulation (cluster D) upon AZD treatment or by repression (cluster C) or upregulation (cluster B) upon DBZ treatment, respectively (Figure 19).

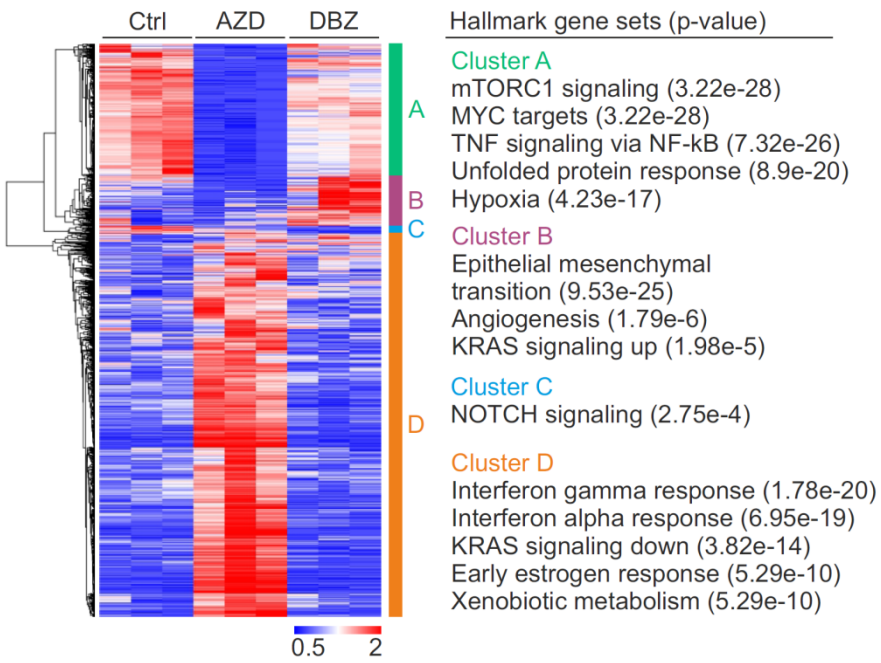

Figure 19. Impact of MAPK and NOTCH repression on gene expression in colon cancer in vivo.

Heat map and unsupervised hierarchical clustering of genes with significantly ($P < 0.05$) differential expression and two or more fold change (left) in SW480 xenografts that were treated for five consecutive days with AZD or DBZ compared with vehicle treatment (Ctrl). Rows represent genes and columns represent n = 3 independent biological replicates. Four main clusters are indicated. Hallmark gene sets most enriched in each cluster as determined by GSEA (right).

Searching for functional associations, we found that genes, which were repressed by AZD treatment (cluster A), were enriched for hallmark gene sets known to be related to MAPK activity, such as mTORC1 signaling or MYC-target genes. Surprisingly however, when characterizing genes that were upregulated by DBZ treatment (cluster B), we found strong enrichment for hallmark gene sets linked to tumor progression and, most significantly, to EMT (Figure 19). GSEA analyses on unfiltered RNA-Seq data of DBZ-treated xenograft tumors confirmed a highly significantly enriched expression of EMT hallmark genes (Figure 20 A).

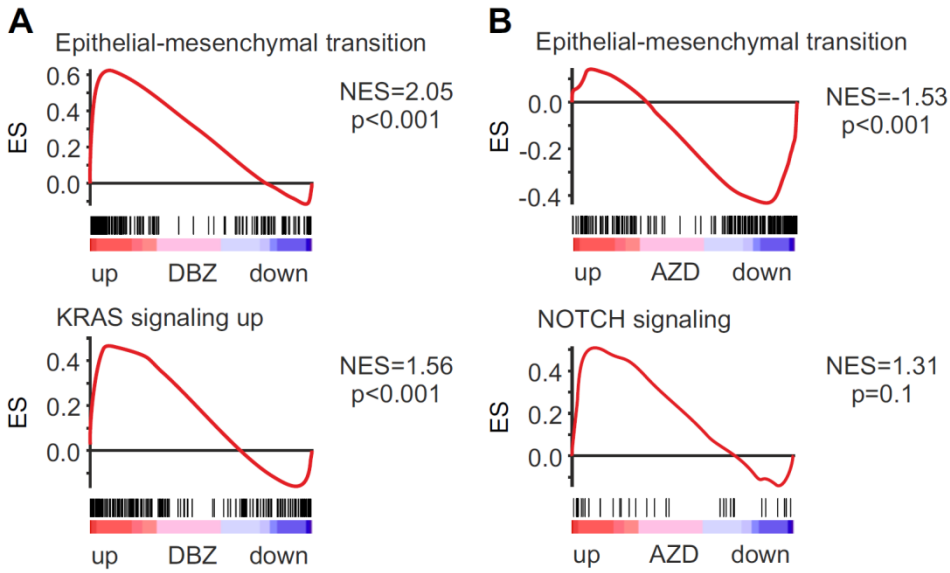

Figure 20. GSEA analyses on DBZ- and AZD-treated colon cancers in vivo.

(A and B) GSEA for indicated gene sets using unfiltered gene expression data of DBZ- (A) and AZD-treated (B) tumors compared with controls. ES, enrichment score; NES, normalized enrichment score. n = 3 independent biological replicates.

On the contrary, when analyzing data from AZD-treated tumors, we found that EMT-related genes were strongly repressed (Figure 20 B). At the same time, NOTCH repression by DBZ caused overexpression of genes related to KRAS signaling (Figure 20 A), whereas MAPK repression with AZD marginally upregulated genes of NOTCH signaling (Figure 20 B).

Because these data suggested opposing effects of MAPK and NOTCH repression on EMT, we next looked at individual factors that were linked to EMT in colon cancer. *ZEB1/2*, *SNAI1/2*, and *TWIST*, which encode for well-known key EMT regulators, but also *VIM*, which indicates an EMT phenotype, showed significantly higher expression levels in DBZ than in AZD treated xenografts (Figure 21 A).

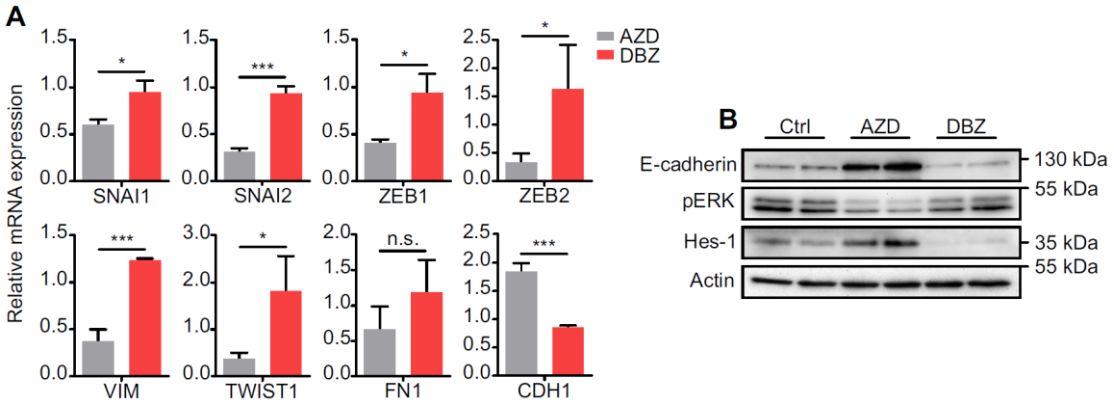

Figure 21. Effects of MAPK and NOTCH repression on EMT in colon cancer xenografts.

(A) Relative expression levels of selected EMT-related genes in SW480 xenografts after 5 d of treatment with AZD or DBZ. Data are mean and error bars indicate SD. n = 3 independent biological replicates. **(B)** Immunoblotting for indicated proteins on tumor lysates of SW480 xenografts after 5 d of vehicle (Ctrl), AZD, or DBZ treatment. n ≥ 3 independent biological replicates, 2 of which are shown. *, $P < 0.05$; ***, $P < 0.001$ by t test; n.s., not significant.

In addition, *CDH1*, which encodes for E-cadherin and indicates epithelial differentiation, was repressed by DBZ and upregulated by AZD. By immunoblotting, we confirmed overexpression of E-cadherin upon AZD treatment on the protein level, although it was reduced in DBZ-treated tumors (Figure 21 B). Also, immunostaining showed strongly increased and expanded E-cadherin expression in tumor cells of SW480 and PDX1 xenografts after AZD treatment, whereas, on the contrary, DBZ treatment reduced E-cadherin levels in these tumors (Figure 22).

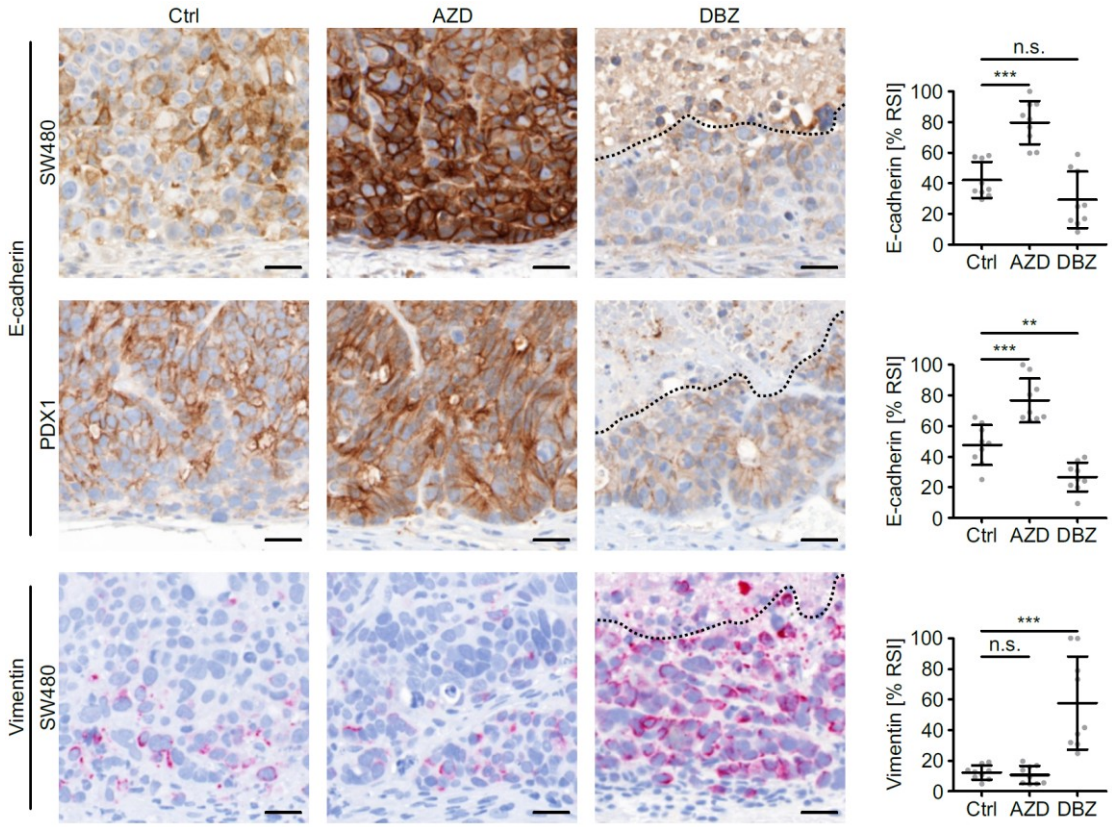

Figure 22. Immunostaining of EMT markers in DBZ- and AZD-treated colon cancers xenografts.

Representative immunostainings (left) and quantification of relative staining intensities (% RSI, right) for E-cadherin and Vimentin in SW480 and/or PDX1 xenografts after 5 d of vehicle (Ctrl), AZD, or DBZ treatment. Areas above dotted lines are tumor necrosis. Scale bars, 25 µm. Error bars are mean ± SD. **, $P < 0.01$; ***, $P < 0.001$ by t test; n.s., not significant. n ≥ 3 independent biological replicates.

Furthermore, tumor cells of SW480 xenografts became strongly positive for Vimentin after DBZ treatment (Figure 22), whereas PDX1 tumors did not express detectable Vimentin levels. Collectively, these data demonstrated that MAPK and NOTCH repression had opposing effects on epithelial differentiation in colon cancer, with NOTCH repression causing an overall shift toward an EMT phenotype.

5.5 Plasticity of MAPK and NOTCH signaling in colon cancer cells

To further learn about the dynamics of tumor cell subpopulations with active MAPK and NOTCH signaling, we developed a lentiviral Cre recombinase–sensitive system for lineage tracing in colon cancer xenografts (Figure 23 A).

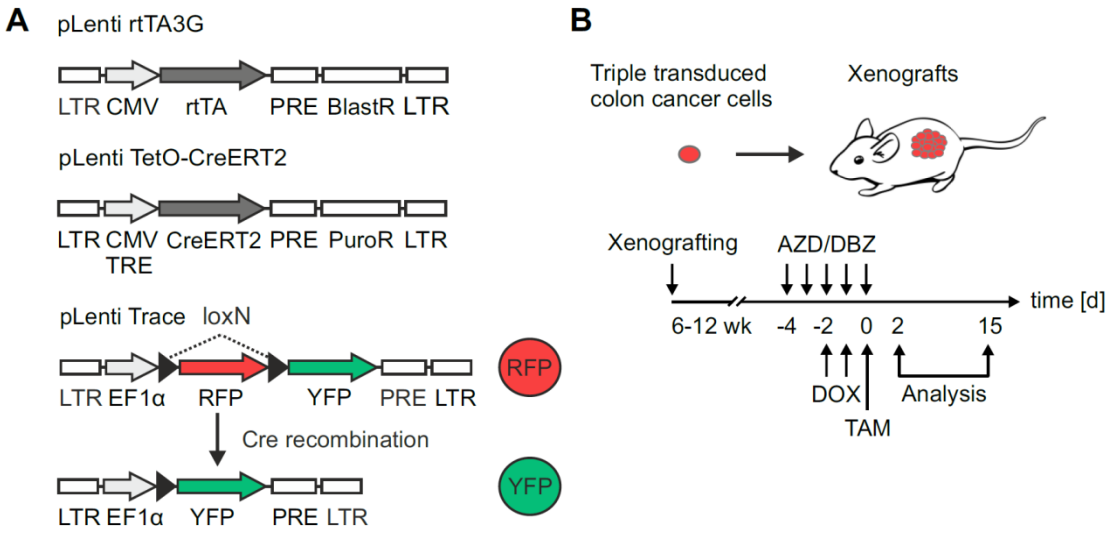

Figure 23. Lentirviral Cre recombinase-sensitive system for lineage tracing and experimental schedule.

(A) Lentiviral vectors for expression of rtTA (pLenti rtTA3G), doxycycline dependent CreERT2 (pLenti TetO-CreERT2), and the Cre-responsive color transgene (pLenti Trace). Upon Cre recombination, the RFP transgene element flanked by loxN will be removed, causing an irreversible switch from expression of RFP to YFP fluorescence. BlastR/PuroR, blasticid and puromycin resistance genes; LTR, long terminal repeat; PRE posttranscriptional regulatory element; TRE, tetracycline response element. **(B)** Triple transduced colon cancer cells were xenografted into NOD/SCID mice. Experimental schedule for Cre recombination by doxycycline (DOX) and tamoxifen (TAM) in AZD- or DBZ-treated xenografts.

This system consists of three lentiviral vectors, two of which mediate doxycycline-inducible expression of an estrogen receptor Cre fusion protein (pLenti rtTA3G and pLenti TetO-CreERT2), and a third vector that upon Cre recombination irreversibly switches from expression of RFP to YFP (pLenti Trace). We transduced all three vectors into SW480 colon cancer cells and xenografted them into immune-compromised NOD/SCID mice. Tumor-bearing mice then were treated with AZD or DBZ, causing loss of FRA1- or NICD-positive tumor cell subpopulations, respectively. Vehicle-treated tumors were included as controls. During treatment and in non-treated controls, recombination was then induced with doxycycline and tamoxifen (Figure 23 B). 2 d after recombination, we observed that individual or small clusters of tumor cells had been labeled by YFP in all xenograft tumors (Figure 24).

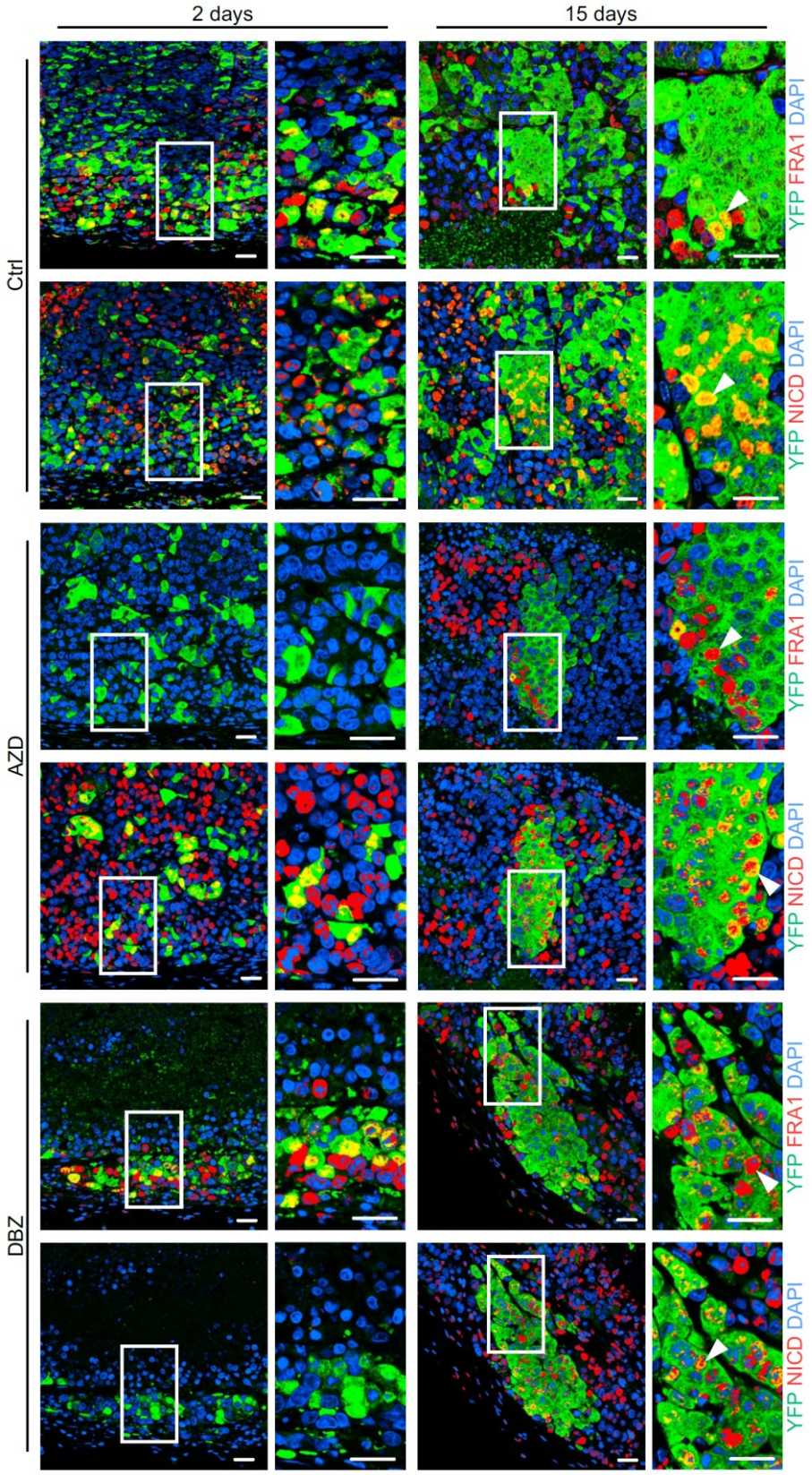

Figure 24. Lineage tracing of colon cancer cells after vehicle treatment, and MAPK or NOTCH inhibition.

Representative double immunofluorescence images for YFP, FRA1, and NICD at 2 and 15 d after recombination in vehicle-, AZD- and DBZ-treated SW480 xenografts, as indicated. Narrow panels are higher magnifications of areas boxed in squared panels. Arrowheads point to FRA1- and NICD-positive tumor cells within single YFP-positive clones at 15 d after recombination. Scale bars, 25 µm.

Importantly, in AZD-treated tumors, the frequency of NICD-/YFP-double positive tumor cells was significantly higher than in non-treated controls, whereas FRA1-positive tumor cells were completely absent (Figure 25 A).

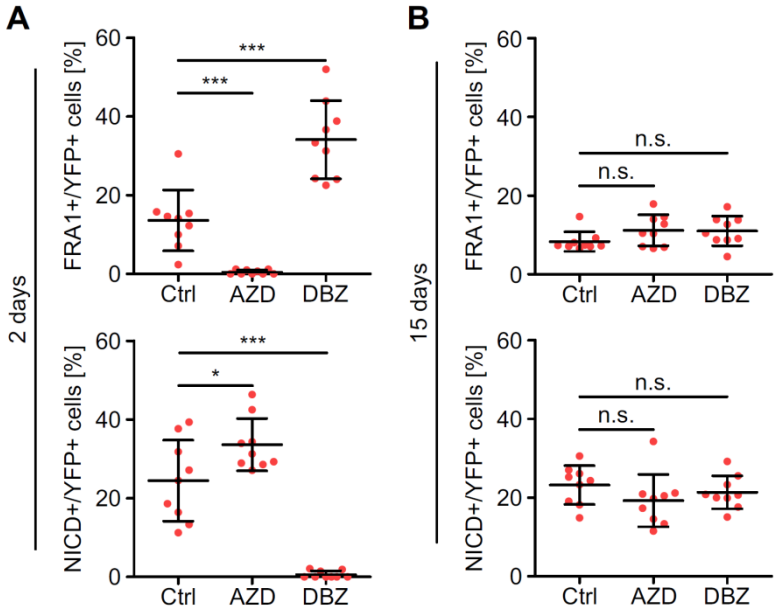

Figure 25. Quantification of colon cancer cell-lineage tracing after vehicle treatment, and MAPK or NOTCH inhibition.

(A and B) Quantification of FRA1-/YFP- and NICD-/YFP-double positive tumor cells in vehicle- (Ctrl), AZD-, and DBZ-treated SW480 xenografts at 2 d (A) and 15 d (B) after recombination. Error bars are mean ± SD. *, $P < 0.05$; ***, $P < 0.001$ by t test; n.s., not significant. n ≥ 3 independent biological replicates.

However, DBZ-treated xenografts had higher frequencies of FRA1-/YFP-double positive tumor cells than control tumors, but contained no NICD-positive tumor cells (Figure 25 A). 15 d after recombination, and after mice had been taken off treatment, we found that clonal patches of YFP-positive tumor cells then had formed, which in all xenografts included both FRA1- and NICD-positive tumor cell subpopulations (Figure 24). Importantly, the frequencies of FRA1-/YFP- and NICD-/YFP-double positives were then similar to those in non-treated control tumors (Figure 25 B).

We also treated PDX1 xenograft tumors with AZD or DBZ and then labeled remaining NICD- or FRA1-positive tumor cells, respectively, with BrdU (Figure 26).

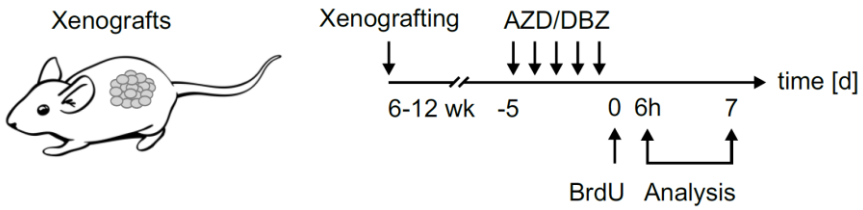

Figure 26. Experimental setup for BrdU pulse labeling.

Schema and experimental schedule for BrdU pulse labeling and chasing in patient-derived PDX1 colon cancer xenografts that were treated with AZD or DBZ.

Analyzing tumors 7 d after AZD or DBZ treatment revealed that the label then had expanded to reappeared FRA1- or NICD-positive tumor cells which at the time of labeling were absent from the tumor (Figure 27).

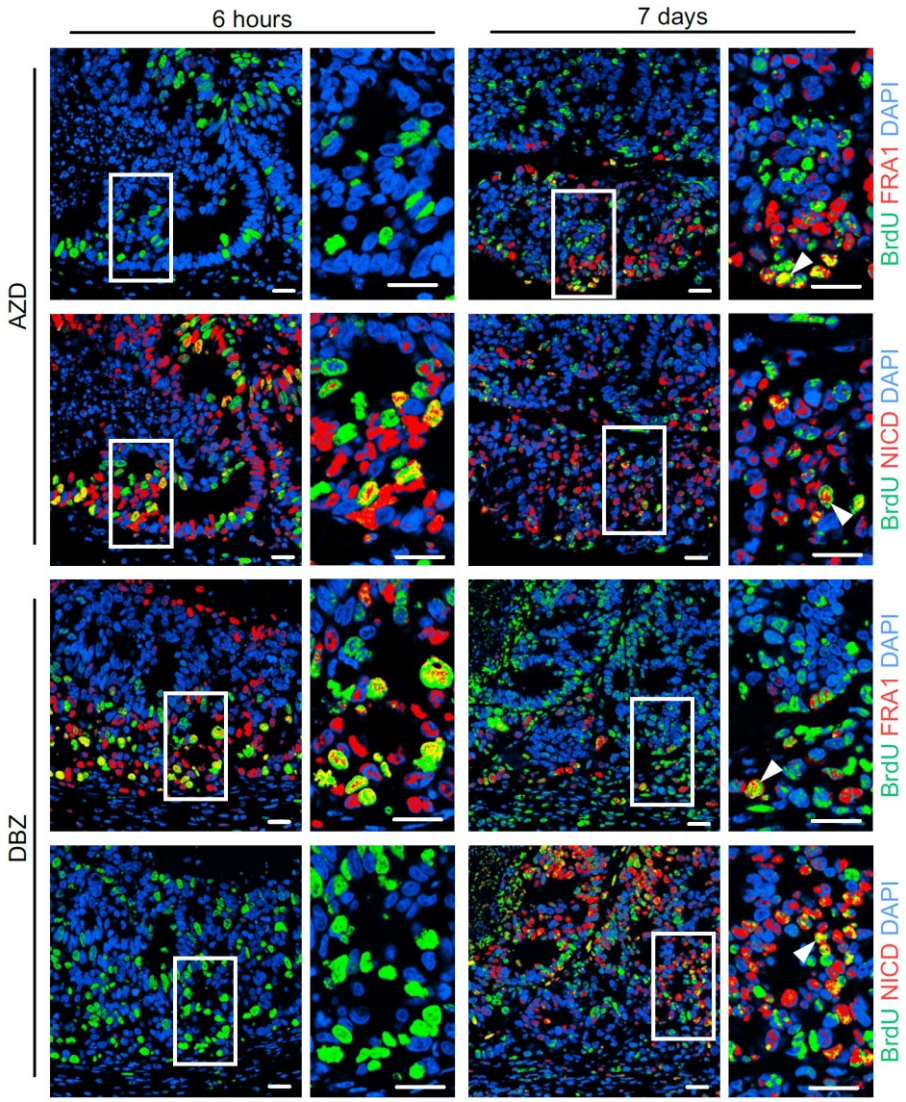

Figure 27. BrdU tracing of colon cancer cells after MAPK and NOTCH inhibition.

Double immunofluorescence for BrdU, FRA1, and NICD at indicated time points after BrdU pulse labeling. Arrowheads in right panels point to BrdU staining in reappeared FRA1- and NICD-positive tumor cells at 7 d. Narrow panels are higher magnifications of areas boxed in squared panels. Representative data from more than three biological replicates are shown. Scale bars, 25 µm.

Furthermore, the frequencies of NICD-/BrdU- and FRA1-/BrdU-double positive tumor cells in AZD- and DBZ-treated tumors, respectively, were higher at 6 h after labeling than at 7 d, where they showed similar frequencies, irrespective of the precedent treatment (Figure 28).

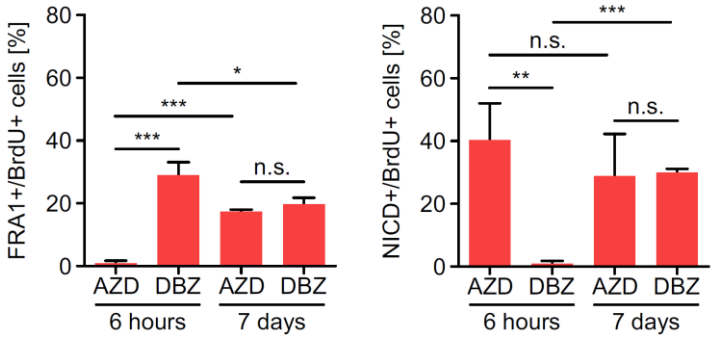

Figure 28. Quantification of colon cancer cell BrdU tracing after MAPK and NOTCH inhibition.

Quantification of FRA1-/BrdU- and NICD-/BrdU-double positive tumor cells in AZD- and DBZ-treated SW480 xenografts at indicated time points after BrdU pulse labeling. Data are mean and error bars indicate SD. *, $P < 0.05$; **, $P < 0.01$; ***, $P < 0.001$ by t test; n.s., not significant. n ≥ 3 independent biological replicates.

Collectively, these findings demonstrate that tumor cell subsets with high MAPK or NOTCH activity can be restored from remaining tumor cells during recovery from AZD or DBZ treatment and provide evidence for plasticity of signaling pathway activity in colon cancer cells.

5.6 Treatment effects of MAPK and NOTCH repression in colon cancer

Finally, we evaluated the effects of targeting MAPK and NOTCH activity on tumor growth and survival in colon cancer xenografts. We applied AZD, DBZ, or a combination of both at treatment intervals of 3 d for several weeks. In addition to SW480 and PDX1, we included cell line-derived SW1222 and patient-derived PDX2 colon cancer xenografts, both of which also had the distribution of FRA1- and NICD-positive tumor cell subpopulations described above. We then evaluated tumor growth over time and observed that AZD treatment significantly slowed tumor growth of PDX2 tumors only, although it had no significant effects on growth of SW480, SW1222, and PDX1 xenografts (Figure 29).

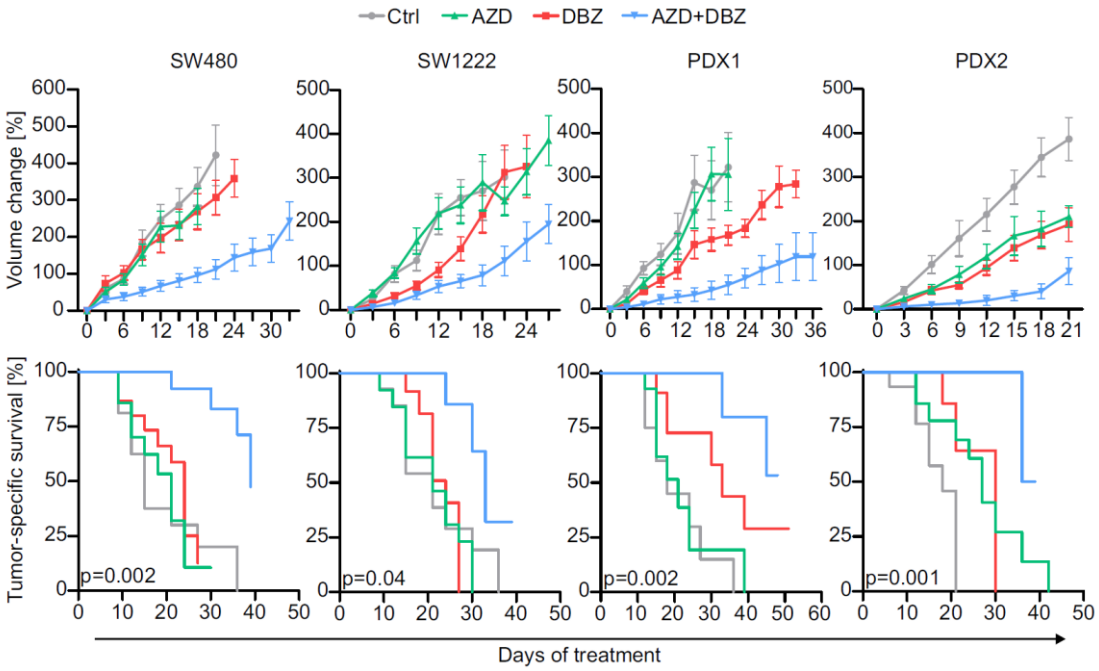

Figure 29. Therapeutic targeting of MAPK and NOTCH in colon cancer xenografts.

Long-term treatment effects of AZD, DBZ, their combination, or vehicle (Ctrl) on SW480-, SW1222-, and patient-derived (PDX1 and PDX2) colon cancer xenografts, shown as growth curves (upper panels) and tumor specific survival in Kaplan-Meier plots (lower panels). Data are mean ± SE in growth curves. *P*-values are log-rank test results in Kaplan-Meier plots. n ≥ 10 independent biological replicates for each treatment group.

Similarly, DBZ treatment slowed tumor growth in PDX2 tumors and also slightly in PDX1 tumors, whereas no overall effects on SW480 and SW1222 were observed. However, combined treatment with AZD and DBZ significantly slowed tumor growth and prolonged tumor-specific survival in all xenograft models, outweighing the effects

of single agent treatments (Figure 29). We then examined treated tumors and found that double treatments strongly reduced proliferation rates, as indicated by Ki67 staining, whereas single agent treatments had no significant effects on proliferation (Figure 30, A and B).

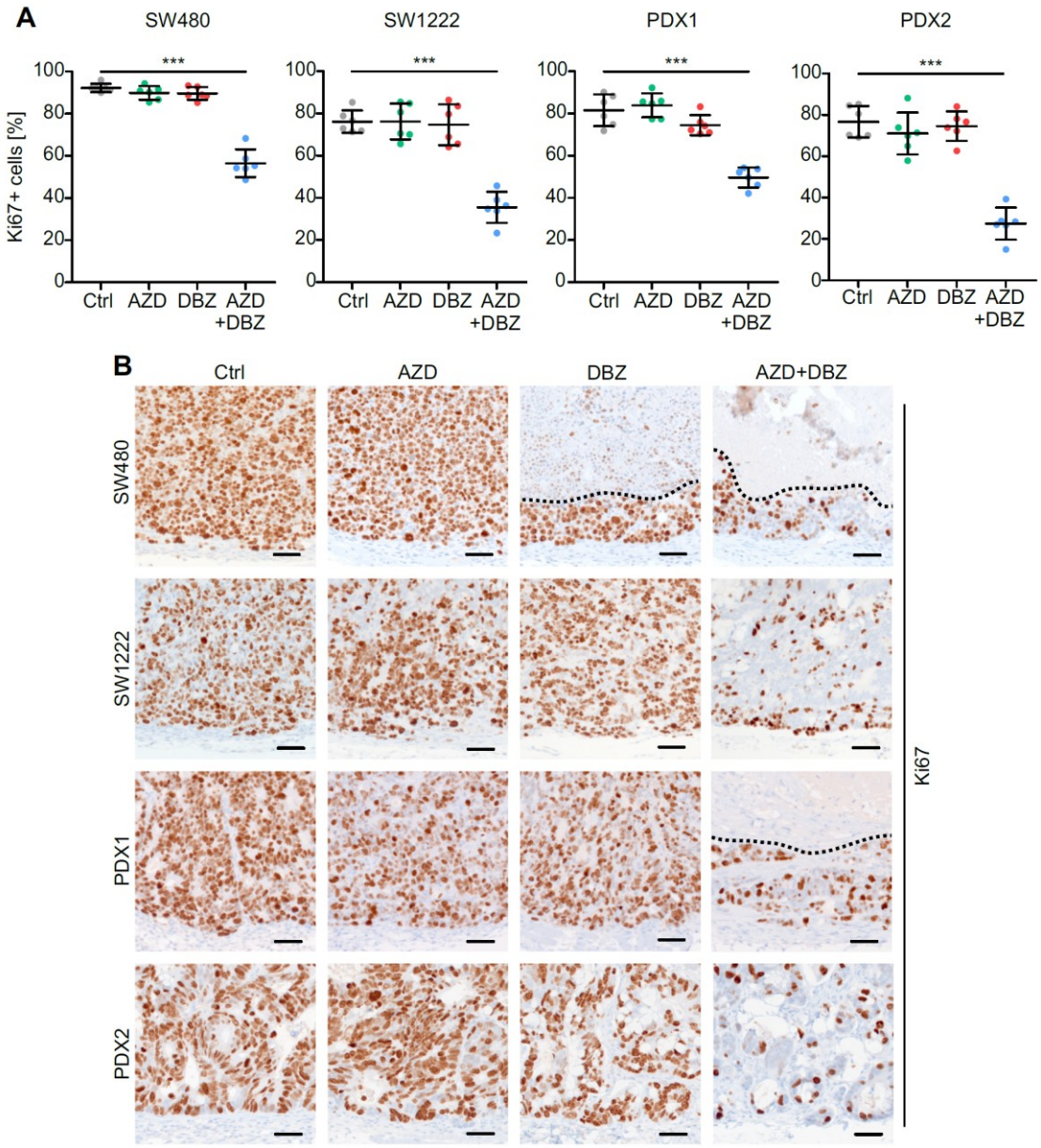

Figure 30. Impact of long-term MAPK and NOTCH repression on proliferation in colon cancer xenografts.

(A) Quantification of immunostaining for Ki67 proliferation index in long-term treated xenografts with AZD, DBZ, their combination, or vehicle (Ctrl). Error bars are mean ± SD. ***, $P < 0.001$ by t test. $n \geq 3$ independent biological replicates. **(B)** Representative immunostainings of Ki67 in SW480-, SW1222-, and patient derived-PDX1 and PDX2 colon cancer xenografts after indicated long-term treatments. Scale bars, 50 µm.

Moreover, double treatment strongly increased apoptosis, as indicated by cleaved Caspase-3, whereas single agent treatments again had lower or no significant effects (Figure 31, A and B).

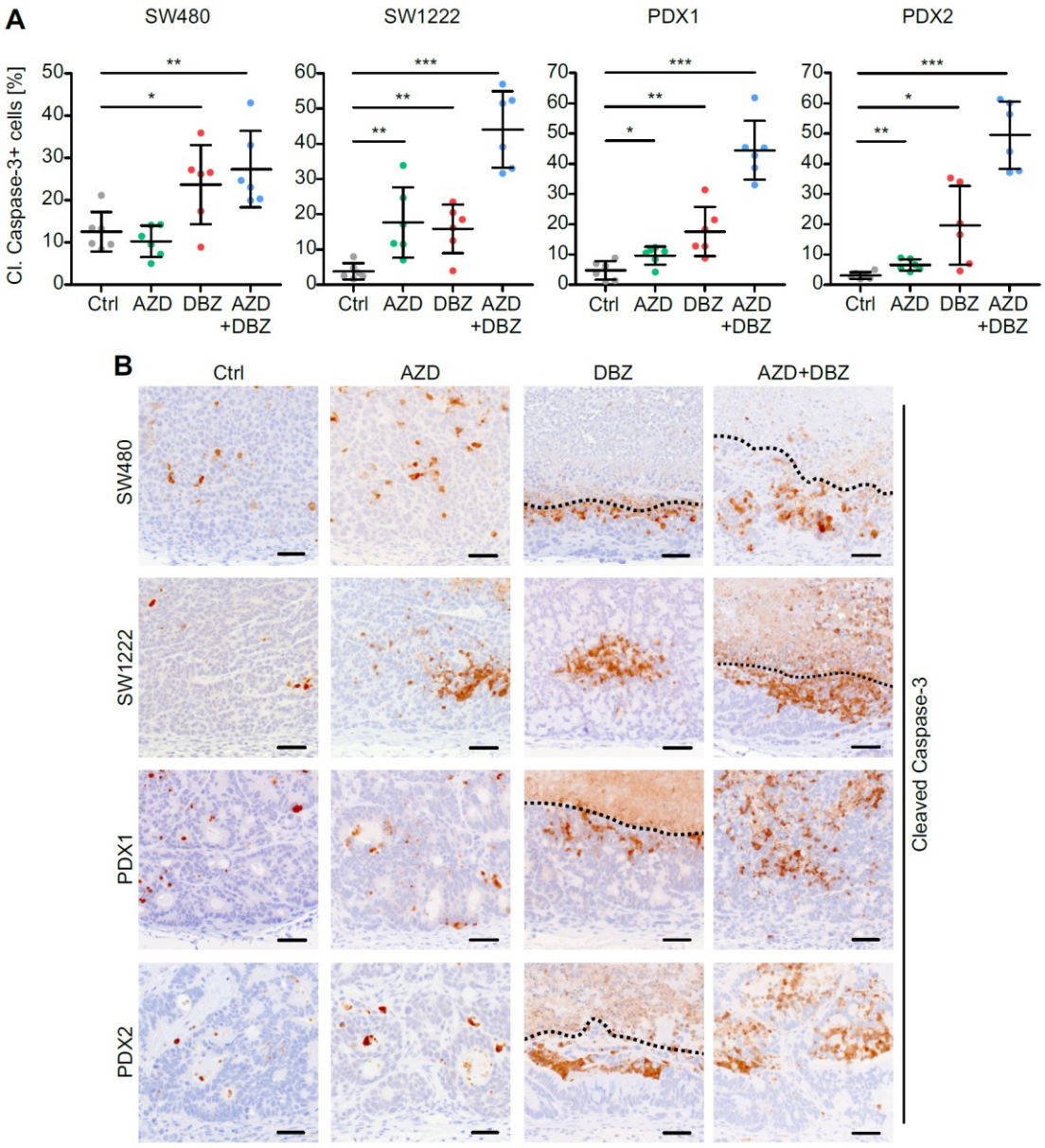

Figure 31. Impact of long-term MAPK and NOTCH repression on apoptosis in colon cancer xenografts.

(A) Quantification of immunostaining for cleaved (Cl.) Caspase-3 in in long-term treated xenografts with AZD, DBZ, their combination, or vehicle (Ctrl). Error bars are mean ± SD. *, $P < 0.05$; **, $P < 0.01$; ***, $P < 0.001$ by t test. n ≥ 3 independent biological replicates. **(B)** Representative immunostainings of cleaved Caspase-3 in SW480-, SW1222-, and patient derived-PDX1 and PDX2 colon cancer xenografts after indicated long-term treatments. Scale bars, 50 µm.

All tumors formed areas of tumor necrosis which variably increased upon treatment. The most significant increase was seen in SW1222 and PDX2 tumors upon double treatment (Figure 32, A and B).

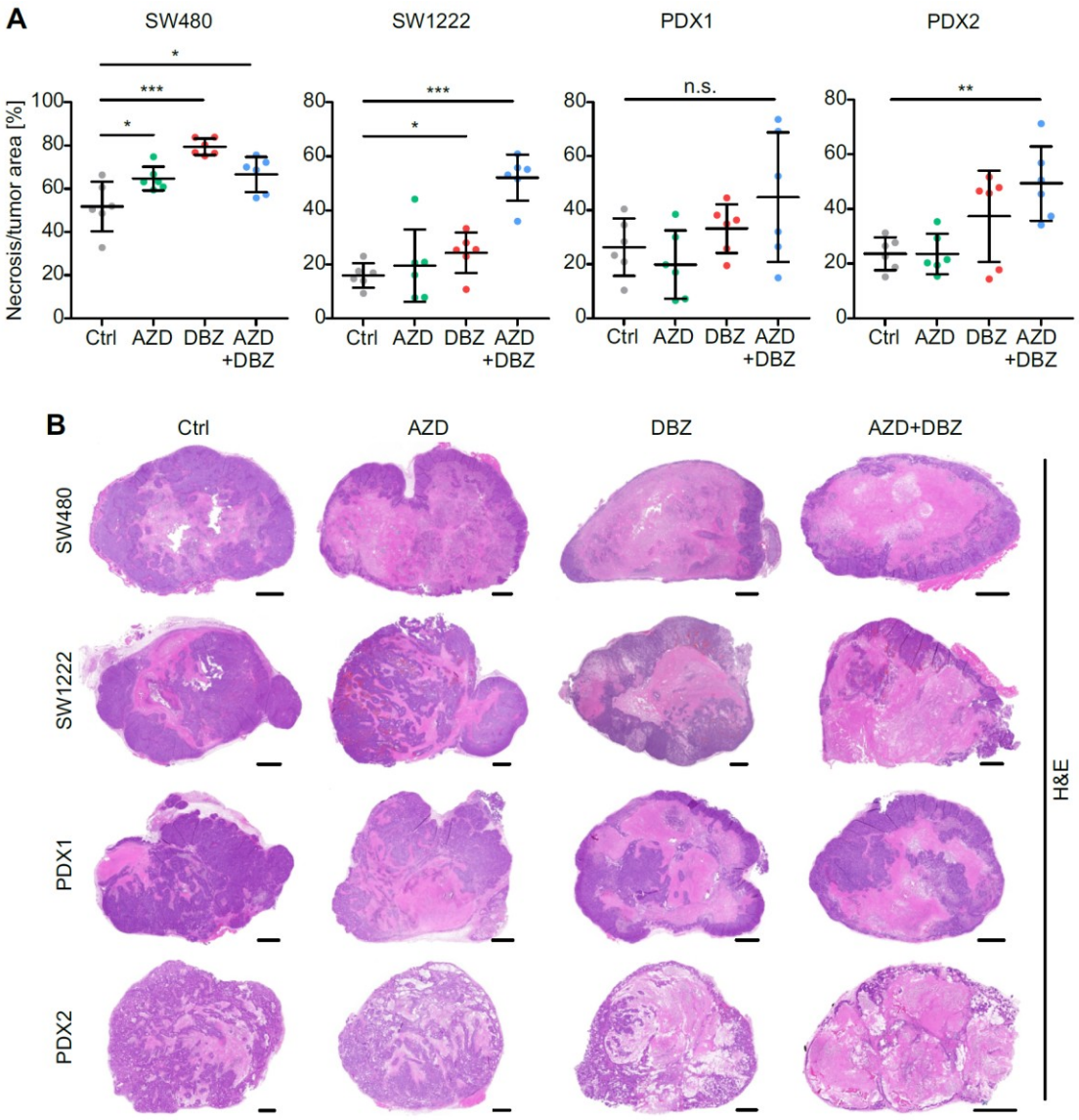

Figure 32. Treatment effects of MAPK and NOTCH repression on necrosis in colon cancer xenografts

(A) Quantification of necrosis in SW480, SW1222, PDX1, and PDX2 colon cancer xenografts after long-term treatment with AZD and/or DBZ or vehicle (Ctrl) as indicated. Error bars are mean ± SD. *, $P < 0.05$; **, $P < 0.01$; ***, $P < 0.001$ by t test; n.s., not significant. n ≥ 3 independent biological replicates. **(B)** Representative overview micrographs of H&E-stained sections of xenograft tumors after indicated long-term treatments. Scale bars, 1 mm.

Of note, however, when analyzing double-treated xenograft tumors for FRA1 and NICD, we observed some remaining positive tumor cells for both markers, suggesting incomplete blockage of MAPK and NOTCH signaling with our treatment protocol (Figure 33).

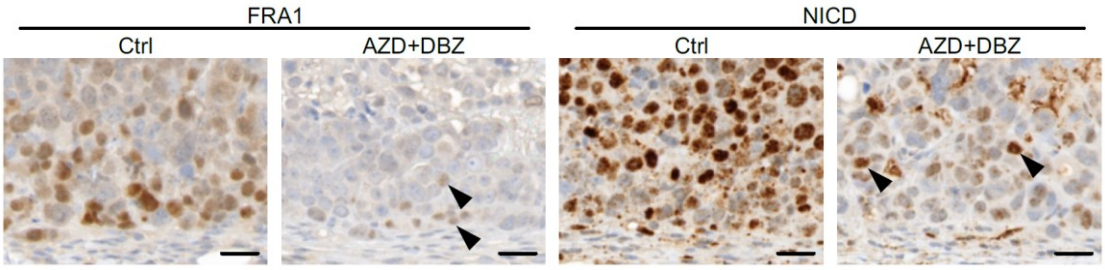

Figure 33. Immunostaining of FRA1 and NICD after long-term double treatment.

Representative immunostainings for FRA1 and NICD in SW480 xenografts after long-term treatment with vehicle (Ctrl), or AZD and DBZ. Arrowheads indicate remaining FRA1- and NICD-positive tumor cells. Scale bars, 25 µm.

Collectively, these data demonstrate superior therapeutic effects upon combined targeting of different tumor cell subpopulations with high MAPK and high NOTCH signaling in colon cancer.

6 DISCUSSION

This work demonstrates that in CRC high NOTCH-signaling activity marks tumor cells with low levels of MAPK and WNT activity, and vice versa indicating that high pathway activities for NOTCH and MAPK/WNT in colon cancer cells are mutually exclusive. Additionally, these pathway activities were linked to distinct tumor cell phenotypes and thus contribute to intratumoral heterogeneity of colorectal cancers [22,26]. While tumor cells with high MAPK activity resided at the tumor edge and underwent EMT, we found that tumor cells with high NOTCH activity had a pronounced epithelial phenotype and were located in the tumor center (Figure 34 A). On one hand, these findings can be explained when considering recent data that showed a repressive role of NOTCH on MAPK and WNT signaling [72,141], both of which are strong inducers of EMT in colon cancer [26,90]. On the other hand, our findings are unexpected in light of previous studies that suggested induction of EMT by NOTCH in various cancer types [68,142–144]. However, in contrast to these data that were mostly derived from cell culture experiments *in vitro* or from other tumor entities, such as lung or breast cancer, we here assessed the distribution of NOTCH activity in primary colon cancer tissues *in situ*. We therefore suggest that the emergence of colon cancer cell subpopulations with full NOTCH activation, their distribution within the tumor as well as the associated epithelial phenotype depend on tumor entity and require the three-dimensional architecture of growing *in vivo*. Therapeutic targeting of colon cancer cells with high MAPK or NOTCH activity by MEK or γ-secretase inhibitors caused a loss of respective tumor cell subpopulations in colon cancer xenografts (Figure 34, B and C).

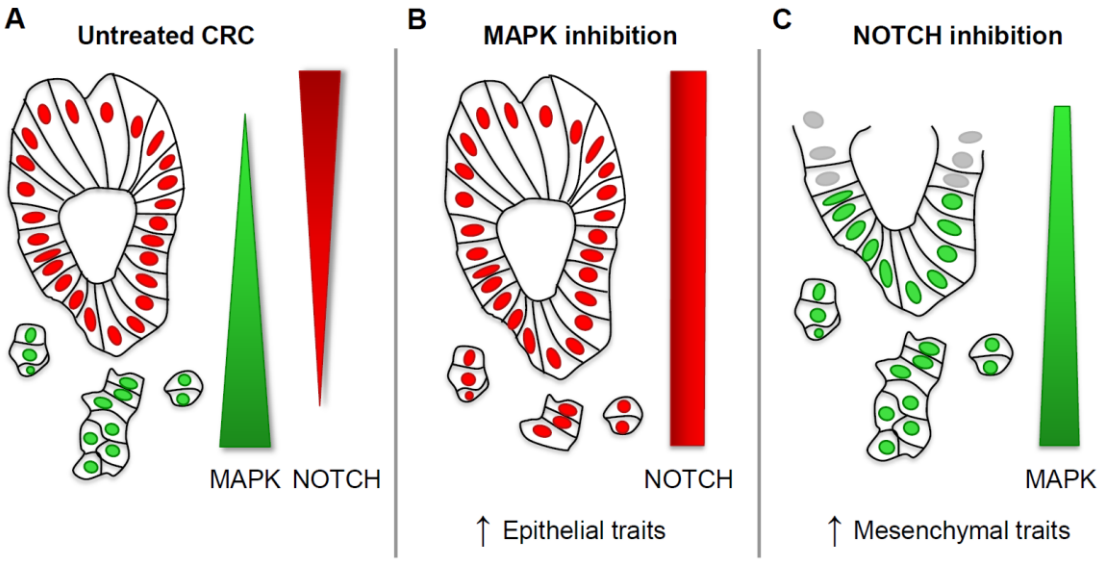

Figure 34. Treatment effects of MAPK and NOTCH inhibition on intratumoral heterogeneity and EMT in CRC.

(A) Intratumoral distribution of tumor cells with active MAPK and NOTCH signaling in CRC. Tumor cells with high MAPK activity are located at the infiltrative tumor edge and underwent EMT. NOTCH signaling is active in tumor cells in the tumor center, revealing epithelial traits. **(B)** Upon repression of MAPK signaling, using a MEK inhibitor, MAPK activity within the tumor is erased, while the NOTCH-active tumor cell subpopulation is expanded. Simultaneously, epithelial traits, indicating MET, are increased. **(C)** Upon NOTCH inhibition, using a γ-secretase inhibitor, tumor cells with high MAPK activity were unaffected or even expanded with a concurrent increase in mesenchmymal features, indicating EMT.

Furthermore, we demonstrate that tumor cells with high MAPK activity were unaffected or even expanded when targeting NOTCH (Figure 34 C), while the NOTCH-active tumor cell population expanded when targeting MAPK signaling (Figure 34 B). These shifts in predominating pathway activity were accompanied by changes in tumor cell phenotypes. Upon NOTCH repression, gene expression and protein levels indicated strongly increased EMT, whereas MAPK repression had opposite effects. Since MAPK is a strong driver of EMT in colon cancer [26,145,146], the elimination of tumor cell subsets with high MAPK activity may induce the shift towards an epithelial phenotype in colon cancer xenografts. Additionally, it was already shown *in vitro* that MEK inhibition as well as FRA1 depletion suppress mesenchymal features and induce differentiation in colorectal cancer cells [42,122,147]. When further considering that EMT is a hallmark of cancer progression [16], we propose that solely targeting NOTCH may elicit limited or even adverse effects on the risk of tumor progression for patients with colon cancer. Our data therefore imply that single agent therapies that target specific signaling pathways require careful evaluation due to

unexpected effects on overall tumor cell differentiation. Furthermore, single agent therapies may cause transitions into potentially aggressive tumor cell populations with intrinsically treatment-resistant phenotypes, often characterized by an EMT-associated gene expression profile [77,148].

Upon recovery from therapy, colon cancer cells with high MAPK or NOTCH activity, respectively, were quickly replenished. Using genetic and BrdU lineage tracing, we demonstrate clonal outgrowth of MAPK- and NOTCH-positive tumor cells from the remaining tumor cell population irrespective of the pathway that was targeted, indicating phenotypic plasticity in signaling pathway activity as an underlying mechanism for treatment recovery. In line with these findings, a recent study demonstrated prompt reappearance of LGR5-positive colon cancer cells after their genetic ablation in tumor xenografts, indicating that tumor cell plasticity allowed reversion of differentiated tumor cells into colon cancer stem cells [103]. In this context, it remains to be determined, if colon cancer cells which express LGR5 or other putative cancer stem cell markers reside within MAPK- and/or NOTCH-positive tumor cell subpopulations. Beside the plasticity between cancer stem cells and differentiated tumor cells [103,104], the reversibility of the EMT program might further support the phenotypic plasticity between distinct tumor cell subpopulations [77,79]. Upon MAPK repression, for instance, MAPK-positive tumor cells associated with a mesenchymal phenotype may shift into NOTCH-positive tumor cells with epithelial features through MET. During recovery from MAPK repression, in turn, the reactivation of EMT in the remaining NOTCH-positive tumor cell subpopulation may induce the reappearance of MAPK-positive tumor cells. Hence, these data suggest that solely targeting colon cancer cell subpopulations with distinct phenotypes, such as EMT or enhanced stemness [77], may clinically fail due to plasticity of phenotype and signaling pathway activity.

Indeed, when we treated colon cancer xenografts for several weeks with MAPK or NOTCH inhibitors alone, effects on tumor growth either were non-significant or moderate only, which is in line with their limited effects in previous therapeutic trials [123,133]. However, when combining both therapies, we found strong repressive effects on tumor cell proliferation and increased apoptosis, resulting in slowed tumor growth and prolonged tumor-specific survival. In melanomas, for instance, similar antitumor activities were obtained upon combined repression of NOTCH and MAPK signaling [149,150]. Given that combinatorial therapies significantly outweighed those of single agent treatments, our findings denote that in CRC combined treatments mainly succeeded by restricting tumor cell plasticity. Furthermore, therapeutic targeting of active EMT in tumors to induce differentiation and epithelial features is discussed as a promising strategy in anticancer treatment [74,76,77]. By contrast, our data indicate that combined inhibition of signaling pathways active in EMT as well as MET phenotypes ultimately revealed improved antitumor efficacy. This lends support to a new concept for cancer therapy which advocates targeting of intratumoral heterogeneity by simultaneous repression of different tumor cell subpopulations to strongly improve therapy response. Detailed analyses of targetable phenotypes and pathways found in different tumor cell subpopulations may thus pave the way for improved treatment options for patients with colorectal and other cancers.

The contribution of colon cancer cell subpopulations to tumor progression is not yet completely understood, however, our data shed useful light on the clinical relevance of MAPK and NOTCH activity. Cancer progression requires invasion and dissemination of tumor cells, which are strongly driven by EMT [78]. However, it also requires seeding at metastatic sites which depends on MET [73]. Because we demonstrate that MAPK and NOTCH activity are linked to EMT and MET phenotypes, respectively, both pathways likely foster colon cancer progression in concert. This idea finds support in our observation that combined analyses of MAPK

and NOTCH activity through FRA1 and NICD was most discriminatory in predicting patient outcome and tumor metastasis. Importantly however, since patients whose tumors showed low activity for both pathways survived best and showed lowest tumor progression and metastasis rates, this further strengthened the rationale for combined targeted treatment against both pathways. As immunostainings for FRA1 and NICD readily indicated presence and extent of respective tumor cell subpopulations in colon cancer specimens, and also often were consistent in primary colon cancers and their metastases, these may well be evaluated as predictive biomarkers. The stratification of CRC patients according to FRA1 and NICD expression in future clinical trials, might help to identify patients that benefit from combinatorial therapies with MEK and γ-secretase inhibitors [27,49]. Consequently, the clinical efficacy of targeted therapies against MAPK- and NOTCH-pathway activities might be predicted by the use of FRA1 and NICD in biomarker-based approaches [27,30,49,151].

In addition to predictive biomarkers, the classification of CRCs based on gene expression profiles may contribute to better clinical stratification [121,152]. Recently, four consensus molecular subtypes (CMSs) of CRC with different features have been proposed. CRCs with subtype CMS2, for instance, reveal epithelial features, whereas CSM4 CRCs have a mesenchymal phenotype that is characterized by increased expression of EMT-associated genes. Additionally, tumors with mixed features exist, possibly indicating intratumoral heterogeneity [152]. Moreover, CRCs of the mesenchymal CMS4 subtype are associated with poor prognosis and may not respond well to adjuvant chemotherapy [148]. Hence, colorectal cancers revealing active MAPK and NOTCH signaling should be further characterized on gene expression levels to determine the CMS subtype [152]. Based on our data, MAPK and NOTCH signaling are associated with mesenchymal and epithelial traits in CRC, respectively. Thus, tumors with heterogeneous MAPK and NOTCH pathway activity

might represent a mixed CMS subtype that could be targeted specifically by a combinatorial therapeutic approach with MEK inhibitors and γ-secretase inhibitors.

Hence, we here provide evidence that combined targeting of MAPK and NOTCH signaling can improve therapeutic response in preclinical xenograft models of CRC. However, this study has certain limitations. Our data are derived from immune-compromised animals which partially lack the inflammatory microenvironment and tumor-directed immune response, so that treatment effects in human patients with CRC may significantly differ. Moreover, since several substances for MAPK and NOTCH inhibition are clinically evaluated [49,112], most tolerable and effective drug combinations in human patients still remain to be determined. Toxic side effects, especially of combined MAPK and NOTCH inhibition also need to be thoroughly assessed. Finally, while long-term repression of MAPK and NOTCH signaling significantly slowed tumor growth, blockage of both pathways was incomplete, and also this treatment failed to regress established tumors. Further preclinical and clinical trials may therefore reveal if combined MAPK and NOTCH inhibition in addition to established chemotherapeutic protocols can improve therapy response in patients with CRC.

SUMMARY

In CRC, signaling pathways driving tumor progression are promising targets for systemic therapy. Besides WNT and MAPK signaling that are active in tumor cells at the infiltrative tumor edge and associated with EMT, activation of NOTCH signaling is found in most tumors. Here we demonstrate that high NOTCH activity marks a distinct colon cancer cell subpopulation, which is located in the tumor center and shows low levels of WNT and MAPK activity as well as a pronounced epithelial phenotype. Therapeutic targeting of MAPK signaling in colon cancer xenografts had limited effects on tumor growth, caused expansion of tumor cells with high NOTCH activity, and promoted epithelial traits. Upon targeting of NOTCH signaling, on the contrary, tumor cells with high MAPK activity and an enhanced EMT phenotype prevailed. Lineage tracing experiments indicated high plasticity between both tumor cell subpopulations as a mechanism for treatment resistance. Combined targeting of NOTCH and MAPK had superior therapeutic effects on colon cancer growth *in vivo*. In CRC case collections, active MAPK and NOTCH signaling was associated with tumor progression, whereas their combined evaluation was most discriminatory in predicting patient outcome and tumor metastasis. Collectively, these findings provide a rationale for combinatorial therapeutic targeting of MAPK and NOTCH signaling in CRC. Targeting different tumor cell subpopulations may reduce treatment resistance by tumor cell plasticity.

ZUSAMMENFASSUNG

Signalwege, die zur Tumorprogression von Kolonkarzinomen beitragen, gelten als vielversprechende Angriffspunkte zielgerichteter Therapieansätze. Eine Vielzahl von Tumoren weist neben einer erhöhten Aktivität des WNT und des MAPK Signalwegs, eine Überaktivierung des NOTCH Signalweges auf. Der WNT und MAPK Signalweg sind in Tumorzellen aktiv, die einen mesenchymalen Phänotyp aufweisen und an der Invasionsfront der Tumoren lokalisiert sind. In dieser Arbeit konnte gezeigt werden, dass Tumorzellen mit einer erhöhten NOTCH Signalwegaktivität eine niedrige Aktivität des WNT und MAPK Signalwegs aufweisen und im Kolonkarzinom eine eigene Tumorzellsubpopulation darstellen. Diese ist im Tumorzentrum lokalisiert und weist epitheliale Eigenschaften auf. Die Effekte einer zielgerichteten Therapie gegen den MAPK Signalweg in Kolonkarzinomxenotransplantaten waren gering und führte zu einer Zunahme von Tumorzellen mit erhöhter NOTCH Signalwegaktivität. Bei der Inhibierung des NOTCH Signalwegs wiederum, blieben Tumorzellen mit erhöhter MAPK Aktivität übrig, die den Phänotypen einer epithelial-mesenchymalen Transition zeigten. Mit Hilfe von „Lineage-tracing“ Experimenten konnte gezeigt werden, dass beide Tumorzellsubpopulationen plastisch ineinander übergehen können. Eine Kombinationstherapie gegen den NOTCH und MAPK Signalweg konnte das Wachstum von Kolonkarzinomxenotransplantaten deutlich reduzieren. In Patientenkollektiven mit Kolonkarzinomen konnte gezeigt werden, dass MAPK und NOTCH Signalwegaktivität, vor allem jedoch die Aktivität beider Signalwege kombiniert, mit schlechter Prognose und Metastasierung von Patienten assoziiert sind. Aus dieser Arbeit lässt sich daher ein neuer kombinierter Therapieansatz ableiten, der sich gegen unterschiedliche Tumorzellsubpopulationen mit hoher MAPK und NOTCH Aktivität richtet. Dieses neue Therapiekonzept ermöglicht es offenbar Behandlungsresistenzen beim Kolonkarzinom zu umgehen, die durch Tumorzellplastizität entstehen können.

ABBREVIATIONS

A	ADAM	A disintegrin and metalloproteinase
	AP	Alkaline phosphatase
	AP1	Activator protein 1
	APC	Adenomatous polyposis coli
	AZD	Selumetinib, AZD6244
B	bp	Base pair
	BrdU	Bromodeoxyuridine
	BSA	Bovine serum albumin
C	cDNA	complementary DNA
	CMS	Consensus molecular subtype
	CRC	Colorectal cancer
	CSCs	Cancer stem cells
	Ctrl	Control
D	DAB	3,3'-Diaminobenzidine
	DAPI	4′,6-Diamidin-2-phenylindol
	DBZ	Dibenzazepine
	DMEM	Dulbecco's Modified Eagle Medium
	DMSO	Dimethylsulfoxide
	DNA	Deoxyribonucleic acid
E	E. coli	Escherichia coli
	EGF	Epidermal growth factor
	EGFR	Epidermal growth factor receptor

	EMT	Epithelial-mesenchymal transition
	ERK	Extracellular signal-regulated kinase
	ES	Enrichment score
	EYFP	Enhanced yellow fluorescent protein
F	FBS	Fetal bovine serum
	FDR	False discovery rate
	FGF	Fibroblast growth factor
	FRA1	FOS-related antigen 1
	fwd	Forward
G	GDP	Guanosine diphosphate
	GEO	Gene expression omnibus
	GFP	Green fluorescent protein
	GRB2	Growth factor receptor-bound protein 2
	GSEA	Gene set enrichment analysis
	GTP	Guanosine triphosphate
H	HES	Hairy Enhancer of Split
	HRP	Horseradish peroxidase
	HTCR	Human tissue and cell research
I	i.p.	Intraperitoneal
L	LGR5	Leucine-rich repeat-containing G protein-coupled receptor 5
	LOH	Loss of heterozygosity
M	MAML1	Mastermind-like protein 1
	MAPK	Mitogen-activated protein kinase
	MEK	MAPK kinase

	MET	Mesenchymal-epithelial transition
N	NaCl	Sodium chloride
	NICD	NOTCH intracellular domain
	NES	Normalized enrichment score
	NP40	Nonidet™ P 40 Substitute
P	p.o.	Orally
	PCR	Polymerase chain reaction
	PDX	Patient derived xenograft
R	rev	Reverse
	RFI	Relative fluorescence intensity
	RFP	Red fluorescent protein
	RIPA	Radioimmunoprecipitation assay
	RSI	Relative staining intensity
	rtTA3G	Reverse tetracycline transactivator 3G
S	SDS	Sodium dodecyl sulfate
	SOS	Son of Sevenless
T	TCF4	Transcription factor 4
	TGF-β	Transforming growth factor-β
U	UICC	Union international contre le cancer
V	V	Volt
	VSV-G	Vesicular stomatitis virus G glyoprotein
W	WPRE	Woodchuck hepatitis post-transcriptional regulatory element
Y	YFP	Yellow fluorescent protein

REFERENCES

1. Siegel, R. L., Miller, K. D. & Jemal, A. Cancer Statistics , 2018. *CA Cancer J Clin* **68,** 7–30 (2018).

2. Global Burden of Disease Cancer Collaboration. Global, Regional, and National Cancer Incidence, Mortality, Years of Life Lost, Years Lived With Disability, and Disability-Adjusted Life-years for 32 Cancer Groups, 1990 to 2015; A Systematic Analysis for the Global Burden of Disease Study Global Burden. *JAMA Oncology* **3,** 524–548 (2017).

3. Huxley, R. R. *et al.* The impact of dietary and lifestyle risk factors on risk of colorectal cancer: A quantitative overview of the epidemiological evidence. *Int. J. Cancer* **125,** 171–180 (2009).

4. Fearon, E. R. Molecular Genetics of Colorectal Cancer. *Annu. Rev. Pathol. Mech. Dis.* **6,** 479–507 (2011).

5. Siegel, R. L. *et al.* Colorectal Cancer Statistics , 2017. *CA Cancer J Clin* **67,** 177–193 (2017).

6. Torre, L. A. *et al.* Global Cancer Statistics, 2012. *CA Cancer J Clin* **65,** 87–108 (2015).

7. Kinzler, K. W. & Vogelstein, B. Lessons from Hereditary Colorectal Cancer. *Cell* **87,** 159–70 (1996).

8. Fearon, E. R. & Vogelstein, B. A Genetic Model for Colorectal Tumorigenesis. *Cell* **61,** 759–767 (1990).

9. Hanahan, D. & Weinberg, R. A. The Hallmarks of Cancer. *Cell* **100,** 57–70 (2000).

10. Vogelstein, B. *et al.* Cancer Genome Landscapes. *Science* **339,** 1546–1558 (2013).

11. The Cancer Genome Atlas Network. Comprehensive molecular characterization of human colon and rectal cancer. *Nature* **487,** 330–337 (2012).

12. Vogelstein, B. *et al.* Genetic Alterations during Colorectal-Tumor Development. *N. Engl. J. Med.* **319,** 525–532 (1988).

13. Bos, J. L. *et al.* Prevalence of ras gene mutations in human colorectal cancers. *Nature* **327,** 293–297 (1987).

14. Takaku, K. *et al.* Intestinal Tumorigenesis in Compound Mutant Mice of both Dpc4 (Smad4) and Apc Genes. *Cell* **92,** 645–656 (1998).

15. Miyaki, M. *et al.* Higher frequency of Smad4 gene mutation in human colorectal cancer with distant metastasis. *Oncogene* **18,** 3098–3103 (1999).

16. Hanahan, D. & Weinberg, R. A. Hallmarks of cancer: The next generation. *Cell* **144,** 646–674 (2011).

17. Korinek, V. *et al.* Constitutive Transcriptional Activation by a β-catenin-Tcf Complex in APC-/- Colon Carcinoma. *Science* **275,** 1784–1787 (1997).

18. Harada, N. *et al.* Intestinal polyposis in mice with a dominant stable mutation of the β-catenin gene. *EMBO J.* **18,** 5931–5942 (1999).

19. Clevers, H. Wnt/β-catenin Signaling in Development and Disease. *Cell* **127,** 469–480 (2006).

20. Van de Wetering, M. *et al.* The β-catenin/TCF-4 Complex Imposes a Crypt Progenitor Phenotype on Colorectal Cancer Cells. *Cell* **111,** 241–250 (2002).

21. Radtke, F. & Clevers, H. Self-Renewal and Cancer of The Gut: Two Dides of a Coin. *Science* **307,** 1904–1909 (2005).

22. Brabletz, T. *et al.* Variable β-catenin expression in colorectal cancers indicates tumor progression driven by the tumor environment. *Proc. Natl. Acad. Sci. U. S. A.* **98,** 10356–10361 (2001).

23. Horst, D. *et al.* Differential WNT activity in colorectal cancer confers limited tumorigenic potential and is regulated by MAPK signaling. *Cancer Res.* **72,** 1547–56 (2012).

24. Vermeulen, L. *et al.* Wnt activity defines colon cancer stem cells and is regulated by the microenvironment. *Nat. Cell Biol.* **12,** 468–476 (2010).

25. Cernat, L. *et al.* Colorectal cancers mimic structural organization of normal colonic crypts. *PLoS One* **9,** 4–11 (2014).

26. Blaj, C. *et al.* Oncogenic effects of high MAPK activity in colorectal cancer mark progenitor cells and persist irrespective of RAS mutations. *Cancer Res.* **77,** 1763–1774 (2017).

27. Ciombor, K. K. & Bekaii-Saab, T. Selumetinib for the treatment of cancer. *Expert Opin. Investig. Drugs* **24,** 111–123 (2015).

28. Akinleye, A., Furqan, M., Mukhi, N., Ravella, P. & Liu, D. MEK and the inhibitors: from bench to bedside. *J. Hematol. Oncol.* **6,** 1–11 (2013).

29. Chang, L. & Karin, M. Mammalian MAP kinase signalling cascades. *Nature* **410,** 37–40 (2001).

30. Sebolt-Leopold, J. S. & Herrera, R. Targeting the mitogen-activated protein kinase cascade to treat cancer. *Nat. Rev. Cancer* **4,** 937–947 (2004).

31. Roberts, P. J. & Der, C. J. Targeting the Raf-MEK-ERK mitogen-activated protein kinase cascade for the treatment of cancer. *Oncogene* **26,** 3291–3310 (2007).

32. Lee, S. *et al.* Colorectal tumors frequently express phosphorylated mitogen-activated protein kinase. *APMIS* **112,** 233–238 (2004).

33. Kim, H. J. & Bar-Sagi, D. Modulation of signalling by sprouty: A developing story. *Nat. Rev. Mol. Cell Biol.* **5,** 441–450 (2004).

34. Yeh, T. C. *et al.* Biological characterization of ARRY-142886 (AZD6244), a potent, highly selective mitogen-activated protein kinase kinase 1/2 inhibitor. *Clin. Cancer Res.* **13,** 1576–1583 (2007).

35. Schubbert, S., Shannon, K. & Bollag, G. Hyperactive Ras in developmental disorders and cancer. *Nat. Rev. Cancer* **7,** 295–308 (2007).

36. Downward, J. Targeting RAS signalling pathways in cancer therapy. *Nat. Rev. Cancer* **3,** 11–22 (2003).

37. Zhang, W., Hart, J., McLeod, H. L. & Wang, H. L. Differential expression of the AP-1 transcription factor family members in human colorectal epithelial and neuroendocrine neoplasms. *Am. J. Clin. Pathol.* **124,** 11–19 (2005).

38. Dhillon, A. S. & Tulchinsky, E. FRA-1 as a driver of tumour heterogeneity: a nexus between oncogenes and embryonic signalling pathways in cancer. *Oncogene* **34,** 4421–4428 (2015).

39. Trahey, M. & McCormick, F. A cytoplasmic protein stimulates normal N-ras p21 GTPase, but does not affect oncogenic mutants. *Science* **238,** 542–545 (1987).

40. Scheffzek, K. *et al.* The Ras-RasGAP Complex: Structural Basis for GTPase Its in Activation and Oncogenic Ras Mutants. *Science* **277,** 333–338 (1997).

41. Shirasawa, S., Furuse, M., Yokoyama, N. & Sasazuki, T. Altered Growth of Human Colon Cancer Cell Lines Disrupted at Activated Ki-ras. *Science* **260,** 85–88 (1993).

42. Diesch, J. *et al.* Widespread FRA1-Dependent Control of Mesenchymal Transdifferentiation Programs in Colorectal Cancer Cells. *PLoS One* **9,** 1–11 (2014).

43. Cheruku, H. R. *et al.* Transforming growth factor-β, MAPK and Wnt signaling interactions in colorectal cancer. *EuPA Open Proteomics* **8,** 104–115 (2015).

44. Massagué, J., Blain, S. W. & Lo, R. S. TGFβ Signaling in Growth Control, Cancer, and Heritable Disorders. *Cell* **103,** 295–309 (2000).

45. Symonds, H. *et al.* p53-Dependent Apoptosis Supresses Tumor Growth and Progression in Vivo. *Cell* **78,** 703–711 (1994).

46. Ntziachristos, P., Lim, J. S., Sage, J. & Aifantis, I. From fly wings to targeted cancer therapies: a centennial for notch signaling. *Cancer Cell* **25,** 318–334 (2014).

47. Reedijk, M. *et al.* Activation of Notch signaling in human colon adenocarcinoma. *Int. J. Oncol.* **33,** 1223–1229 (2008).

48. Zhang, Y., Li, B., Ji, Z.-Z. & Zheng, P.-S. Notch1 regulates the growth of human colon cancers. *Cancer* **116,** 5207–18 (2010).

49. Takebe, N. *et al.* Targeting Notch, Hedgehog, and Wnt pathways in cancer stem cells: clinical update. *Nat. Rev. Clin. Oncol.* **12,** 445–464 (2015).

50. Artavanis-Tsakonas, S., Rand, M. D. & Lake, R. J. Notch signaling: cell fate control and signal integration in development. *Science* **284,** 770–776 (1999).

51. Qiao, L. & Wong, B. C. Y. Role of Notch signaling in colorectal cancer. *Carcinogenesis* **30,** 1979–1986 (2009).

52. Bray, S. Notch signalling: a simple pathway becomes complex. *Nat. Rev. Mol. Cell Biol.* **7,** 678–689 (2006).

53. Takebe, N., Harris, P. J., Warren, R. Q. & Ivy, S. P. Targeting cancer stem cells by inhibiting Wnt, Notch, and Hedgehog pathways. *Nat. Rev. Clin. Oncol.* **8,** 97–106 (2011).

54. Ranganathan, P., Weaver, K. L. & Capobianco, A. J. Notch signalling in solid tumours: a little bit of everything but not all the time. *Nat. Rev. Cancer* **11,** 338–351 (2011).

55. Espinoza, I., Pochampally, R., Xing, F., Watabe, K. & Miele, L. Notch signaling: targeting cancer stem cells and epithelial-to-mesenchymal transition. *Onco. Targets. Ther.* **6,** 1249–1259 (2013).

56. Amsen, D., Antov, A. & Flavell, R. A. The different faces of Notch in T-helper-cell differentiation. *Nat. Rev. Immunol.* **9,** 116–124 (2009).

57. Kopan, R. Notch Signaling. *Cold Spring Harb Perspect Biol* **4,** 1–4 (2012).

58. Takebe, N., Nguyen, D. & Yang, S. X. Targeting notch signaling pathway in cancer: clinical development advances and challenges. *Pharmacol. Ther.* **141,** 140–149 (2014).

59. Schroeter, E. H., Kisslinger, J. A. & Kopan, R. Notch-1 signaling requires ligand-induced proteolytic release of intracellular domain. *Nature* **393,** 382–386 (1998).

60. De Strooper, B. *et al.* A presenilin-1-dependet g-secretase-like protease mediates release of Notch intracelluar domain. *Nature* **398,** 518–522 (1999).

61. Wilson, J. J. & Kovall, R. A. Crystal structure of the CSL-Notch-Mastermind Ternary complex bound to DNA. *Cell* **124,** 985–996 (2006).

62. Wu, L. *et al.* MAML1, a human homologue of Drosophila mastermind, is a transcriptional co-activator for NOTCH receptors. *Nat. Genet.* **26,** 484–489 (2000).

63. Fre, S. *et al.* Notch and Wnt signals cooperatively control cell proliferation and tumorigenesis in the intestine. *Proc. Natl. Acad. Sci.* **106,** 6309–6314 (2009).

64. Rodilla, V. *et al.* Jagged1 is the pathological link between Wnt and Notch pathways in colorectal cancer. *Proc. Natl. Acad. Sci.* **106,** 6315–6320 (2009).

65. Guilmeau, S., Flandez, M., Mariadason, J. M. & Augenlicht, L. H. Heterogeneity of Jagged1 expression in human and mouse intestinal tumors: implications for targeting Notch signaling. *Oncogene* **29,** 992–1002 (2010).

66. Bu, P. *et al.* A microRNA miR-34a-regulated bimodal switch targets notch in colon cancer stem cells. *Cell Stem Cell* **12,** 602–615 (2013).

67. Sikandar, S. S. *et al.* NOTCH signaling is required for formation and self-renewal of tumor-initiating cells and for repression of secretory cell differentiation in colon cancer. *Cancer Res.* **70,** 1469–1478 (2010).

68. Fender, A. W., Nutter, J. M., Fitzgerald, T. L., Bertrand, F. E. & Sigounas, G. Notch-1 Promotes Stemness and Epithelial to Mesenchymal Transition in Colorectal Cancer. *J. Cell. Biochem.* **116,** 2517–2527 (2015).

69. Brabletz, S. *et al.* The ZEB1/miR-200 feedback loop controls Notch signalling in cancer cells. *EMBO J.* **30,** 770–782 (2011).

70. Sonoshita, M. *et al.* Suppression of colon cancer metastasis by Aes through inhibition of Notch signaling. *Cancer Cell* **19,** 125–137 (2011).

71. Kim, M., Kim, H. & Yoon, S. Colon cancer progression is driven by APEX1-mediated upregulation of Jagged. *J. Clin. Invest.* **123,** 3211–3230 (2013).

72. Kim, H. *et al.* Notch1 counteracts WNT/ β-catenin signaling through chromatin modification in colorectal cancer. *J. Clin. Invest.* **122,** 3248–3259 (2012).

73. Lamouille, S., Xu, J. & Derynck, R. Molecular mechanisms of epithelial–mesenchymal transition. *Nat. Rev. Mol. Cell Biol.* **15,** 178–196 (2014).

74. Thiery, J. P., Acloque, H., Huang, R. Y. J. & Nieto, M. A. Epithelial-Mesenchymal Transitions in Development and Disease. *Cell* **139,** 871–890 (2009).

75. Tam, W. L. & Weinberg, R. A. The epigenetics of epithelial-mesenchymal plasticity in cancer. *Nat. Med.* **19,** 1438–1449 (2013).

76. Polyak, K. & Weinberg, R. A. Transitions between epithelial and mesenchymal states: acquisition of malignant and stem cell traits. *Nat. Rev. Cancer* **9,** 265–273 (2009).

77. Shibue, T. & Weinberg, R. A. EMT, CSCs, and drug resistance: The mechanistic link and clinical implications. *Nat. Rev. Clin. Oncol.* **14,** 611–629 (2017).

78. Massagué, J. & Obenauf, A. C. Metastatic colonization by circulating tumor cells. *Nature* **529,** 298–306 (2016).

79. Ocaña, O. H. *et al.* Metastatic Colonization Requires the Repression of the Epithelial-Mesenchymal Transition Inducer Prrx1. *Cancer Cell* **22,** 709–724 (2012).

80. Davis, F. M., Stewart, T. A., Thompson, E. W. & Monteith, G. R. Targeting EMT in cancer: opportunities for pharmacological intervention. *Trends Pharmacol. Sci.* **35,** 479–488 (2014).

81. Perl, A. K., Wilgenbus, P., Dahl, U., Semb, H. & Christofori, G. A causal role for E-cadherin in the transition from adenoma to carcinoma. *Nature* **392,** 190–193 (1998).

82. Thiery, J. P. & Sleeman, J. P. Complex networks orchestrate epithelial-mesenchymal transitions. *Nat. Rev. Mol. Cell Biol.* **7,** 131–142 (2006).

83. Batlle, E. *et al.* The transcription factor Snail is a repressor of E-cadherin gene expression in epithelial tumour cells. *Nat. Cell Biol.* **2,** 84–89 (2000).

84. Cano, A. *et al.* The transcription factor Snail controls epithelial-mesenchymal transitions by repressing E-cadherin expression. *Nat. Cell Biol.* **2,** 76–83 (2000).

85. Hajra, K. M., Chen, D. Y. & Fearon, E. R. The SLUG Zinc-Finger Protein Represses E-Cadherin in Breast Cancer. *Cancer Res.* **62,** 1613–1618 (2002).

86. Grooteclaes, M. L. & Frisch, S. M. Evidence for a function of CtBP in epithelial gene regulation and anoikis. *Oncogene* **19,** 3823–3828 (2000).

87. Eger, A. *et al.* DeltaEF1 is a transcriptional repressor of E-cadherin and regulates epithelial plasticity in breast cancer cells. *Oncogene* **24,** 2375–2385 (2005).

88. Comijn, J. *et al.* The Two-handed E Box Binding Zinc Finger Protein SIP1 Downregulates E-Cadherin and Induces Invasion. *Mol. Cell* **7,** 1267–1278 (2001).

89. Gonzalez, D. M. & Medici, D. Signaling mechanisms of the epithelial-mesenchymal transition. *Sci. Signal.* **7,** 1–16 (2014).

90. Sánchez-Tilló, E. *et al.* β-catenin/TCF4 complex induces the epithelial-to-mesenchymal transition (EMT)-activator ZEB1 to regulate tumor invasiveness. *Proc. Natl. Acad. Sci.* **108,** 19204–19209 (2011).

91. Brabletz, T., Jung, A., Spaderna, S., Hlubek, F. & Kirchner, T. Opinion: migrating cancer stem cells - an integrated concept of malignant tumour progression. *Nat. Rev. Cancer* **5,** 744–749 (2005).

92. Pyke, C. *et al.* Laminin-5 Is a Marker of Invading Cancer Cells in Some Human Carcinomas and Is Coexpressed with the Receptor for Urokinase Plasminogen Activator in Budding Cancer Cells in Colon Adenocarcinomas. *Cancer Res.* **55,** 4132–4139 (1995).

93. Visvader, J. E. & Lindeman, G. J. Cancer stem cells in solid tumours: accumulating evidence and unresolved questions. *Nat. Rev. Cancer* **8,** 755–768 (2008).

94. Dalerba, P. *et al.* Phenotypic characterization of human colorectal cancer stem cells. *Proc. Natl. Acad. Sci. U. S. A.* **104,** 10158–10163 (2007).

95. Meacham, C. E. & Morrison, S. J. Tumour heterogeneity and cancer cell plasticity. *Nature* **501,** 328–337 (2013).

96. Marusyk, A., Almendro, V. & Polyak, K. Intra-tumour heterogeneity: A looking glass for cancer? *Nat. Rev. Cancer* **12,** 323–334 (2012).

97. Ricci-Vitiani, L. *et al.* Identification and expansion of human colon-cancer-initiating cells. *Nature* **445,** 111–115 (2007).

98. O'Brien, C. A., Pollett, A., Gallinger, S. & Dick, J. E. A human colon cancer cell capable of initiating tumour growth in immunodeficient mice. *Nature* **445,** 106–110 (2007).

99. Vermeulen, L. *et al.* Single-cell cloning of colon cancer stem cells reveals a multi-lineage differentiation capacity. *Proc. Natl. Acad. Sci.* **105,** 13427–13432 (2009).

100. Schepers, A. G. *et al.* Lineage Tracing Reveals Lgr5+ Stem Cell Activity in Mouse Intestinal Adenomas. *Science* **337,** 730–735 (2012).

101. Driessens, G., Beck, B., Caauwe, A., Simons, B. D. & Blanpain, C. Defining the mode of tumour growth by clonal analysis. *Nature* **488,** 527–530 (2012).

102. Kretzschmar, K. & Watt, F. M. Lineage tracing. *Cell* **148,** 33–45 (2012).

103. Shimokawa, M. *et al.* Visualization and targeting of LGR5+ human colon cancer stem cells. *Nature* **545,** 187–192 (2017).

104. Schwitalla, S. *et al.* Intestinal tumorigenesis initiated by dedifferentiation and acquisition of stem-cell-like properties. *Cell* **152,** 25–38 (2013).

105. Wellner, U. *et al.* The EMT-activator ZEB1 promotes tumorigenicity by repressing stemness-inhibiting microRNAs. *Nat. Cell Biol.* **11,** 1487–1495 (2009).

106. Mani, S. A. *et al.* The Epithelial-Mesenchymal Transition Generates Cells with Properties of Stem Cells. *Cell* **133,** 704–715 (2008).

107. Plaks, V., Kong, N. & Werb, Z. The cancer stem cell niche: How essential is the niche in regulating stemness of tumor cells? *Cell Stem Cell* **16,** 225–238 (2015).

108. Dienstmann, R., Salazar, R. & Tabernero, J. Personalizing colon cancer adjuvant therapy: Selecting optimal treatments for individual patients. *J. Clin. Oncol.* **33,** 1787–1796 (2015).

109. Gill, S. *et al.* Pooled analysis of fluorouracil-based adjuvant therapy for stage II and III colon cancer: Who benefits and by how much? *J. Clin. Oncol.* **22,** 1797–1806 (2004).

110. Gallagher, D. J. & Kemeny, N. Metastatic colorectal cancer: From improved survival to potential cure. *Oncology* **78,** 237–248 (2010).

111. Gonda, T. J. & Ramsay, R. G. Directly targeting transcriptional dysregulation in cancer. *Nat. Rev. Cancer* **15,** 686–694 (2015).

112. Miyamoto, Y., Suyama, K. & Baba, H. Recent Advances in Targeting the EGFR Signaling Pathway for the Treatment of Metastatic Colorectal Cancer. *Int. J. Mol. Sci.* **18,** 1–15 (2017).

113. De Roock, W. *et al.* Effects of KRAS, BRAF, NRAS, and PIK3CA mutations on the efficacy of cetuximab plus chemotherapy in chemotherapy-refractory metastatic colorectal cancer: A retrospective consortium analysis. *Lancet Oncol.* **11,** 753–762 (2010).

114. Yoon, J., Koo, K. H. & Choi, K. Y. MEK1/2 inhibitors AS703026 and AZD6244 may be potential therapies for KRAS mutated colorectal cancer that is resistant to EGFR monoclonal antibody therapy. *Cancer Res.* **71,** 445–453 (2011).

115. Misale, S. *et al.* Emergence of KRAS mutations and acquired resistance to anti-EGFR therapy in colorectal cancer. *Nature* **486,** 532–536 (2012).

116. Karapetis, C. S. *et al.* K-ras Mutations and Benefit from Cetuximab in Advanced Colorectal Cancer. *N. Engl. J. Med.* **359,** 1757–1765 (2008).

117. Van Cutsem, E. *et al.* Cetuximab plus irinotecan, fluorouracil, and leucovorin as first-line treatment for metastatic colorectal cancer: Updated analysis of overall survival according to tumor KRAS and BRAF mutation status. *J. Clin. Oncol.* **29,** 2011–2019 (2011).

118. Lièvre, A. *et al. KRAS* Mutations As an Independent Prognostic Factor in Patients With Advanced Colorectal Cancer Treated With Cetuximab. *J. Clin. Oncol.* **26,** 374–379 (2008).

119. Lièvre, A. *et al.* KRAS mutation status is predictive of response to cetuximab therapy in colorectal cancer. *Cancer Res.* **66,** 3992–3995 (2006).

120. Yoon, H. H. *et al.* KRAS codon 12 and 13 mutations in relation to disease-free survival in BRAF-wild-type stage III colon cancers from an adjuvant chemotherapy trial (N0147 alliance). *Clin. Cancer Res.* **20,** 3033–3043 (2014).

121. Dienstmann, R. *et al.* Consensus molecular subtypes and the evolution of precision medicine in colorectal cancer. *Nat. Rev. Cancer* **17,** 79–92 (2017).

122. Davies, B. R. *et al.* AZD6244 (ARRY-142886), a potent inhibitor of mitogen-activated protein kinase/extracellular signal-regulated kinase kinase 1/2 kinases: mechanism of action in vivo, pharmacokinetic/pharmacodynamic relationship, and potential for combination in preclinical. *Mol. Cancer Ther.* **6,** 2209–2219 (2007).

123. Bennouna, J. *et al.* A Phase II, open-label, randomised study to assess the efficacy and safety of the MEK1/2 inhibitor AZD6244 (ARRY-142886) versus capecitabine monotherapy in patients with colorectal cancer who have failed one or two prior chemotherapeutic regimens. *Invest. New Drugs* **29,** 1021–1028 (2011).

124. Adjei, A. A. *et al.* Phase I pharmacokinetic and pharmacodynamic study of the oral, small-molecule mitogen-activated protein kinase kinase 1/2 inhibitor AZD6244 (ARRY-142886) in patients with advanced cancers. *J. Clin. Oncol.* **26,** 2139–2146 (2008).

125. Miyamoto, S., Nakanishi, M. & Rosenberg, D. W. Suppression of colon carcinogenesis by targeting Notch signaling. *Carcinogenesis* **34,** 2415–2423 (2013).

126. Ghaleb, A. M., Aggarwal, G., Bialkowska, A. B., Nandan, M. O. & Yang, V. W. Notch Inhibits Expression of the Kruppel-Like Factor 4 Tumor Suppressor in the Intestinal Epithelium. *Mol. Cancer Res.* **6,** 1920–1927 (2008).

127. Akiyoshi, T. *et al.* γ-Secretase Inhibitors Enhance Taxane-Induced Mitotic Arrest and Apoptosis in Colon Cancer Cells. *Gastroenterology* **134,** 131–144 (2008).

128. Meng, R. D. *et al.* γ-secretase inhibitors abrogate oxaliplatin-induced activation of the Notch-1 signaling pathway in colon cancer cells resulting in enhanced chemosensitivity. *Cancer Res.* **69,** 573–582 (2009).

129. Chu, D. *et al.* High level of notch1 protein is associated with poor overall survival in colorectal cancer. *Ann. Surg. Oncol.* **17,** 1337–1342 (2010).

130. Yuan, R. *et al.* HES1 promotes metastasis and predicts poor survival in patients with colorectal cancer. *Clin. Exp. Metastasis* **32,** 169–179 (2015).

131. Messersmith, W. A. *et al.* A phase I, dose-finding study in patients with advanced solid malignancies of the oral γ-secretase inhibitor PF-03084014. *Clin. Cancer Res.* **21,** 60–67 (2015).

132. Aung, K. L. *et al.* A multi-arm phase I dose escalating study of an oral NOTCH inhibitor BMS-986115 in patients with advanced solid tumours. *Invest. New Drugs* (2018).

133. Strosberg, J. R. *et al.* A phase II study of RO4929097 in metastatic colorectal cancer. *Eur. J. Cancer* **48,** 997–1003 (2012).

134. Tolcher, A. W. *et al.* Phase I study of RO4929097, a gamma secretase inhibitor of notch signaling, in patients with refractory metastatic or locally advanced solid tumors. *J. Clin. Oncol.* **30,** 2348–2353 (2012).

135. Lamprecht, S. *et al.* Multicolor lineage tracing reveals clonal architecture and dynamics in colon cancer. *Nat. Commun.* **8,** 1–9 (2017).

136. Zufferey, R., Nagy, D., Mandel, R. J., Naldini, L. & Trono, D. Multiply attenuated lentiviral vector achieves efficient gene delivery in vivo. *Nat. Biotechnol.* **15,** 871–874 (1997).

137. Naldini, L., Blomer, U., Gage, F. H., Trono, D. & Verma, I. M. Efficient transfer, integration, and sustained long-term expression of the transgene in adult rat brains injected with a lentiviral vector. *Proc. Natl. Acad. Sci.* **93,** 11382–11388 (1996).

138. Thasler, W. E. *et al.* Charitable state-controlled foundation human tissue and cell research: Ethic and legal aspects in the supply of surgically removed human tissue for research in the academic and commercial sector in Germany. *Cell Tissue Bank.* **4,** 49–56 (2003).

139. Liberzon, A. *et al.* The Molecular Signatures Database Hallmark Gene Set Collection. *Cell Syst.* **1,** 417–425 (2015).

140. Subramanian, A., Tamayo, P. & Mootha, V. Gene set enrichment analysis: A knowledge-based approach for interpreting genome-wide expression profiles. *Proc. Natl. Acad. Sci.* **102,** 15545–15550 (2005).

141. Rampias, T. *et al.* A new tumor suppressor role for the Notch pathway in bladder cancer. *Nat. Med.* **20,** 1199–1205 (2014).

142. Leong, K. G. *et al.* Jagged1-mediated Notch activation induces epithelial-to-mesenchymal transition through Slug-induced repression of E-cadherin. *J. Exp. Med.* **204,** 2935–2948 (2007).

143. Sahlgren, C., Gustafsson, M. V, Jin, S., Poellinger, L. & Lendahl, U. Notch signaling mediates hypoxia-induced tumor cell migration and invasion. *Proc. Natl. Acad. Sci.* **105,** 6392–6397 (2008).

144. Yang, Y. *et al.* The Notch ligand Jagged2 promotes lung adenocarcinoma metastasis through a miR-200-dependent pathway in mice. *J. Clin. Invest.* **121,** 1373–1385 (2011).

145. Bakiri, L. *et al.* Fra-1/AP-1 induces EMT in mammary epithelial cells by modulating Zeb1/2 and TGFβ expression. *Cell Death Differ.* **22,** 336–350 (2015).

146. Lemieux, É. *et al.* Constitutively active MEK1 is sufficient to induce epithelial-to-mesenchymal transition in intestinal epithelial cells and to promote tumor invasion and metastasis. *Int. J. Cancer* **125,** 1575–1586 (2009).

147. Herr, R. *et al.* B-Raf inhibitors induce epithelial differentiation in BRAF-mutant colorectal cancer cells. *Cancer Res.* **75,** 216–229 (2015).

148. Song, N. *et al.* Clinical outcome from oxaliplatin treatment in stage II/III colon cancer according to intrinsic subtypes: Secondary analysis of NSABP C-07/NRG oncology randomized clinical trial. in *JAMA Oncology* **2,** 1162–1169 (2016).

149. Zhu, G. *et al.* Combination with γ-secretase inhibitor prolongs treatment efficacy of BRAF inhibitor in BRAF-mutated melanoma cells. *Cancer Lett.* **376,** 43–52 (2016).

150. Krepler, C. *et al.* Targeting Notch enhances the efficacy of ERK inhibitors in BRAF-V600E melanoma. *Oncotarget* **7,** 71211–71222 (2016).

151. Noah, T. K. & Shroyer, N. F. Notch in the intestine: regulation of homeostasis and pathogenesis. *Annu. Rev. Physiol.* **75,** 263–288 (2013).

152. Guinney, J. *et al.* The consensus molecular subtypes of colorectal cancer. *Nat. Med.* **21,** 1350–1356 (2015).

ACKNOWLEDGMENT

First, I am especially grateful to Prof. Dr. Andreas Jung for giving me the chance to work on this interesting project, for his scientific input and his constant support throughout my doctoral thesis.

I also want to thank Prof. Dr. David Horst for his valuable advices and helpful discussions. Furthermore, I express gratitude to Prof. Dr. Thomas Kirchner for supporting this project. Additionally, I address special thanks to Anja Heier, Andrea Sendelhofert and Jessica Kövi for excellent technical assistance and their support, especially in stressful moments.

Besides, I owe special thanks to all the AG Horst lab members, particularly to Dr. Cristina Blaj and Dr. Sebastian Lamprecht for their support, valuable discussions and our great times in the lab. Thanks are also due to my other colleagues in the institute, who always had a friendly ear, especially to Ursula Götz, Sabine Sagebiel, Gülfem Oener and Dr. Vera Link. I address special thanks to Dr. Markus Kaller for his steady encouragement and the funny moments we shared during the last years.

Additionally, I am especially thankful to all my friends, who accompanied and supported me along the way. Anna and Sabrina, thank you so much for our close and long-lasting friendship since over 20 years.

Above all, I want to express my sincere gratitude to my family, who always believed in me and keeps encouraging me in everything I am doing.

Last but not least, I am deeply grateful to Simon for always being there, all your love, understanding and support. Thank you so much for standing by my side during that chapter in my life.